


Review

Review on Wearable Thermoelectric Generators: From Devices to Applications

Sijing Zhu ¹, Zheng Fan ², Baoquan Feng ¹, Runze Shi ¹, Zexin Jiang ¹, Ying Peng ³, Jie Gao ¹, Lei Miao ^{1,2,*} 
and Kunihito Koumoto ^{4,5,*}

- ¹ Guangxi Key Laboratory of Information Material, School of Material Science and Engineering, Guilin University of Electronic Technology, Guilin 541004, China; zhusj1910@foxmail.com (S.Z.); 21102302011@mails.guet.edu.cn (B.F.); 21102201042@mails.guet.edu.cn (R.S.); 21102201019@mails.guet.edu.cn (Z.J.); nextyeargi@gmail.com (J.G.)
- ² Guangxi Key Laboratory for Relativistic Astrophysics, School of Physical Science and Technology, Guangxi University, Nanning 530004, China; fz15078858467gxu@163.com
- ³ Engineering Research Center of Electronic Information Materials and Devices, Ministry of Education, Guangxi Key Laboratory of Precision Navigation Technology and Application, Guilin University of Electronic Technology, Guilin 541004, China; pengying@guet.edu.cn
- ⁴ Nagoya Industrial Science Research Institute, Nagoya 464-0819, Japan
- ⁵ Center of Nanotechnology, King Abdulaziz University, Jeddah 21589, Saudi Arabia
- * Correspondence: miaolei@guet.edu.cn (L.M.); g44233a@cc.nagoya-u.ac.jp (K.K.)

Abstract: Wearable thermoelectric generators (WTEGs) can incessantly convert body heat into electricity to power electronics. However, the low efficiency of thermoelectric materials, tiny terminal temperature difference, rigidity, and neglecting optimization of lateral heat transfer preclude WTEGs from broad utilization. In this review, we aim to comprehensively summarize the state-of-the-art strategies for the realization of flexibility and high normalized power density in thermoelectric generators by establishing the links among materials, TE performance, and advanced design of WTEGs (structure, heatsinks, thermal regulation, thermal analysis, etc.) based on inorganic bulk TE materials. Each section starts with a concise summary of its fundamentals and carefully selected examples. In the end, we point out the controversies, challenges, and outlooks toward the future development of wearable thermoelectric devices and potential applications. Overall, this review will serve to help materials scientists, electronic engineers, particularly students and young researchers, in selecting suitable thermoelectric devices and potential applications.

Keywords: wearable thermoelectric generators; power density; inorganic bulk TE materials; thermal analysis; wearable devices



Citation: Zhu, S.; Fan, Z.; Feng, B.; Shi, R.; Jiang, Z.; Peng, Y.; Gao, J.; Miao, L.; Koumoto, K. Review on Wearable Thermoelectric Generators: From Devices to Applications. *Energies* **2022**, *15*, 3375. <https://doi.org/10.3390/en15093375>

Academic Editor: Bertrand Lenoir

Received: 1 March 2022

Accepted: 28 April 2022

Published: 5 May 2022

Publisher's Note: MDPI stays neutral with regard to jurisdictional claims in published maps and institutional affiliations.



Copyright: © 2022 by the authors. Licensee MDPI, Basel, Switzerland. This article is an open access article distributed under the terms and conditions of the Creative Commons Attribution (CC BY) license (<https://creativecommons.org/licenses/by/4.0/>).

1. Introduction

In the past few decades, with the advancement of nanomaterials and microelectronics technology, small-sized, low-power-consuming, and multifunctional electronic devices, especially wearable devices, have experienced rapid development. Examples include electronic skin and wristbands that can monitor human physiological data. In addition, the integration of these devices with the Internet of Things (IoT) has also attracted a lot of attention, especially for communication systems, environmental monitoring, and biomedical devices [1–5]. This integration allows devices to be equipped with wireless connectivity to directly transmit data from various sensors to a cloud diagnostic server for further analysis. For example, a portable electrocardiogram (ECG) system can monitor the heart data of patients with heart disease and remind medical staff to take action once arrhythmia occurs [6,7]. Smart wearable devices, such as intelligent clothes that monitor temperature and air parameters, can alert personnel who are exposed to toxic or substandard air conditions, thus enabling swift evacuation. However, these devices require laborious, non-stop measuring of parameters. Lately, soft and durable batteries, such as

environmentally friendly water-zinc batteries [8] and lithium sulfide batteries [9,10], have also been developed as power sources for electronic devices. However, most batteries either need to be replaced regularly or need to be recharged. The limited lifespan and the need for frequent replacement further weaken the functionality of wearables. For example, in 24-h health monitoring applications, rechargeable batteries are undesirable because the operation may be interrupted during charging. This can lead to a severe lack of data availability and hamper medical treatment. Targeting this issue, self-powered devices that facilitate continuous monitoring of data over longer periods of time have become a popular direction of research in recent years. An adult can generate more than 100 W through activities such as breathing, heating, blood transport, and walking [11]. Therefore, merely converting 1% of the energy produced by the human body into electricity is sufficient to support the operation of most portable electronic devices [12–14]. Various energy harvesting technologies, such as triboelectric generators (TEGs) [15–17], piezoelectric generators [18], and thermoelectric generators (TEGs) [19–21], have been developed to convert human biomechanical energy (from human movement and body temperature) into electricity. However, triboelectric generators (TEGs) and piezoelectric generators are unstable in terms of energy harvesting from the human body. While body heat is the main energy source of human metabolism and is a constant heat source, thermoelectric generators (TEGs) can provide permanent DC power for electronic devices by collecting and converting body heat without noise and maintenance. Nevertheless, achieving an efficiency of 1% is more challenging than expected, as TEGs only cover a small part of the human body, so wearable thermoelectric generators are required to maximize efficiency. The maximization requires the precise design of TEGs at the material, device, and system levels. The most direct and effective way of enhancing efficiency is to improve the ZT of TE materials. At present, inorganic TE materials represented by bismuth telluride can reach a ZT of 2.2 at room temperature [22]. Organic materials represented by PEDOT:PSS [23–26] also appear as promising candidates because of their good flexibility. However, the highest ZT of the most advanced organic materials could not exceed 0.75 [22]. In addition, thin-film materials/devices exhibit high ZT and power density [27,28], but their large-area heat collection is unsatisfactory. The WTEGs based on inorganic bulk have the most potential as power sources for wearable electronic devices because of their high output and are discussed in this paper. Figure 1 shows the overview of WTEGs in this review. We introduce the trends in wearable technology and the basic concepts of WTEG in Sections 1 and 2. The optimization strategies based on inorganic bulk WTEGs, including TE materials and thermal management, are summarized in Section 3. Section 4 discusses the markets of WTEG and various WTEGs-driven devices related to wearable health monitoring sensors and environmental monitoring. Section 5 describes existing challenges while predicting future trends of WTEG.

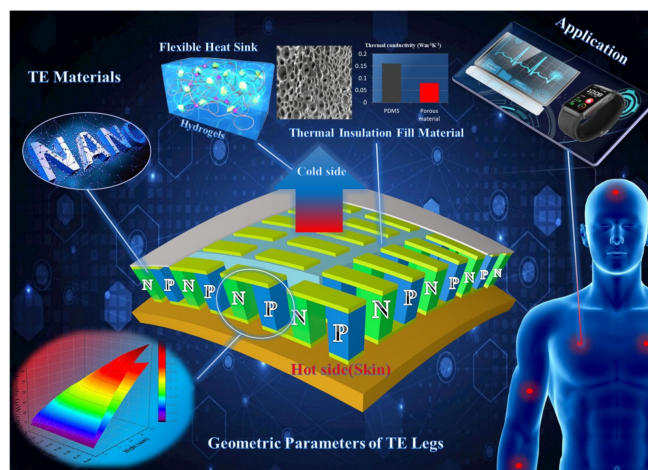


Figure 1. A schematic diagram showing the structure, optimization strategy, and applications of WTEG.

2. Thermoelectric Generators

2.1. Basic Concept of Thermoelectric Generators

Commonly, the thermoelectric effect first includes the Seebeck effect, which was discovered in 1821 by Estonian physicist Thomas Johann Seebeck, and the Peltier effect and Thomson effect, discovered by Peltier in 1834 and Thomson in 1851, respectively. Different metals (or semiconductors) have different free electron densities. When two different metals (or semiconductors) are in contact with each other (Figure 2A), the electrons on the contact surface will diffuse to eliminate the difference in electron density. A stable voltage is generated at the other end of the metals (or semiconductors), and the diffusion rate of electrons is proportional to the temperature of the contact area. The same metal (or semiconductor) at different temperatures also has different free electron densities, so as long as the temperature difference between the two ends of the metal is maintained, the electrons can continue to diffuse, and an open-circuit voltage is generated at both ends of the metal (or semiconductor) called Seebeck voltage (V), as given in Equation (1) [29,30].

$$V = S \times \Delta T \quad (1)$$

where S and ΔT are the Seebeck coefficient and temperature difference, respectively. The practical TE conversion efficiency of a TEG is given by the following Equation (2):

$$\eta = \frac{P}{Q_h} \quad (2)$$

where P is the power output to the load (output energy), and Q_h is the heat energy absorbed at the hot side (input energy). Theoretically, the maximum energy conversion efficiency depends only on the temperature difference of the device and the intrinsic ZT of the TE material, as Equations (3) and (4) show [31]:

$$\eta_{max} = \frac{T_h - T_c}{T_h} \frac{\sqrt{1 + ZT_{avg}} - 1}{\sqrt{1 + ZT_{avg}} + \frac{T_c}{T_h}} \quad (3)$$

$$T_{avg} = \frac{T_h + T_c}{2} \quad (4)$$

where T_h is the temperature of the hot side of the TEG, T_c is that of its cold side, and $(T_h - T_c / T_h)$ is the maximum efficiency of the Carnot cycle. T_{avg} is the average temperature. ZT_{avg} is evaluated by the following equation, Equation (5) [31]:

$$ZT_{avg} = \frac{S^2 \sigma}{\kappa} \times T_{avg} \quad (5)$$

where σ and κ represent the electrical conductivity and thermal conductivity, respectively. To obtain high TE conversion efficiency, high ZT is required. Meanwhile, to elevate ZT_{avg} , the σ and S values should be large, and the κ value ought to be small. However, σ , S , and κ are strongly coupled through the carrier concentration (n) [32]. In other words, it is challenging to tune σ , S , and κ independently, hence realizing high ZT_{avg} is not within easy reach.

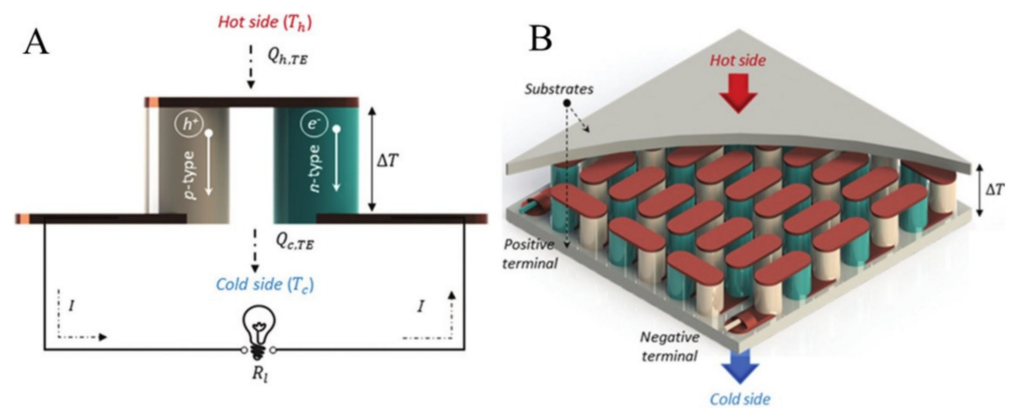


Figure 2. Schematic diagrams of the (A) Seebeck effect [22]. (B) TEG module [22].

A typical TEG module consists of pairs of π -type TE legs connected in series, as shown in Figure 2B. Based on the Seebeck effect, each pair of π -type TE legs consists of the p-type and n-type semiconductors fixed in series between two insulating substrates. When a heat source of temperature T_h is applied onto one side of the TEG, and another side of the TEG is exposed to a low temperature (T_c) environment, a temperature difference (ΔT) is created between the TE pair. Therefore, most of the charge carriers generated at p-type (holes) TE legs and n-type (electrons) TE legs move from the higher to the lower temperature side, which generates an open-circuit voltage (V_{oc}) across these TE pairs [33,34]. The electrical energy generated by a module depends on the number of thermocouples, the thermocouple geometry, TE properties of the thermocouple material, the thermal and electrical properties of the contact layers, electrodes, substrates, and the temperature difference. To simplify the evaluation, we assume that the absolute value of the Seebeck coefficient and the thermal and electrical conductivities of the p-type and n-type TE materials are equal.

The produced power (P) on the load resistance (R_L) connected to a TEG module is given by:

$$P = \frac{V^2}{(R_{TEG} + R_L)^2} \times R_L \quad (6)$$

where R_{TEG} is the internal resistance of TEG. When the load resistance (R_L) is equal to R_{TEG} , the maximum power (P_{max}) is obtained:

$$P_{max} = \frac{V_{oc}^2}{4 \times R_{TEG}} \quad (7)$$

The V_{oc} produced by a TEG module and the R_{TEG} can be evaluated by Equations (8) and (9) [35]:

$$V_{oc} = \frac{NS(T_h - T_c)}{1 + 2r_{th}L_c/L} \quad (8)$$

$$R_{TEG} = 2N \frac{\rho(r_e + L)}{A} \quad (9)$$

where N is the number of TE couples, and A and L are the cross-sectional area and length of TE legs, respectively, and L_c is the thickness of the contact layer. Next, there is $r_e = \rho_c/\rho$ and $r_{th} = \lambda_c/\lambda$ (where ρ_c is the electrical contact resistivity, λ_c is the thermal contact conductivity, and ρ and λ are the electrical resistivity and thermal conductivity of TE materials, respectively). r_e and r_{th} are usually referred to as the electrical and thermal contact parameters, respectively. For commercially TEG modules, appropriate values are $r_e \sim 0.1$ and $r_{th} \sim 0.2$.

The maximum power (P_{max}) is obtained as [35]:

$$P_{max} = \frac{S^2}{2\rho} \times \frac{AN(T_h - T_c)^2}{(r_e + L)\left(1 + \frac{2r_{th}L_c}{L}\right)^2} \quad (10)$$

The maximum energy conversion efficiency (η_{max}) is obtained as [35]:

$$\eta_{max} = \frac{\left(\frac{T_H - T_C}{T_H}\right)}{\left(1 + \frac{2r_{th}L_c}{L}\right)^2 \left[2 - \frac{1}{2}\left(\frac{T_H - T_C}{T_H}\right) + \left(\frac{4}{ZT_H}\right)\left(\frac{L + r_e}{L + 2r_{th}L_c}\right)\right]} \quad (11)$$

2.2. Heat Transfer Model of Human Body as Heat Source

The TEG uses the temperature gradient as the driving force, thus enabling its application in aerospace, vehicle, and other fields in which temperature gradients are generated. The TEG module consisting of 36 pairs of bismuth telluride (Bi_2Te_3) was first commercialized by General Electric in 1959 [36]. Because the human body can act as a stable heat source, wearable thermoelectric generators have been developed to drive wearable electronic devices. When the TEG is worn on the human body, the thermal system becomes complicated due to the thermal contact resistance and different environments (Air velocity, ambient temperature). Figure 3A shows a schematic for the heat transfer model of a wearable thermoelectric generator. The heat flows from the skin through the TEG to the air. Note that the temperature difference between the two ends of the TEG ($\Delta T_{int} = T_h - T_c$) is not the temperature difference between the human skin and the environment ($\Delta T_{ext} = T_s - T_a$) but is estimated by the following equation, Equation (12) [37]:

$$\Delta T_{int} = (T_h - T_c) = (T_s - T_a) \times \frac{R_{th,g}}{R_{th,h} + R_{th,g} + R_{th,c}} \quad (12)$$

where T_a is the ambient temperature, T_s is the temperature of the human skin, and $R_{th,h}$, $R_{th,g}$, and $R_{th,c}$ are the thermal resistances of skin contact, TEG, and air convection, respectively. The practical thermal resistance of a TEG is given by Equation (13) [37]:

$$R_{th,g} = \frac{1}{\kappa} \frac{L}{FF \times A_{TEG}} \quad (13)$$

where A_{TEG} is the area of the TEG, FF is the fill factor (the area of TE legs/the area of the WTEGs), κ is the thermal conductivity of the TE material, and L is the height of the thermoelectric legs.

The core temperature of a human body is maintained between 36.5 and 37.5 °C, through thermoregulation [38]. The thermal conductivity of skin has been reported to between 0.26–0.3 W/mK, which is a complex function of specific physiological parameters, such as body weight, age, body fat, and gender [39]. Figure 3B shows the variation of skin temperature relative to air temperature in different parts of the human body [40].

When a TEG is placed on human skin, it is affected by the skin's thermal resistance in addition to the thermal contact resistance at the TEG-skin interface [41,42]. Since the skin itself is a rough surface, air gaps between the TEG and the skin can significantly hinder the heat transfer performance of the TEG. Additionally, since the skin is soft and elastic with pressure, the contact resistance at the skin/TEG interface is highly dependent on the amount of pressure applied. Figure 3C shows the estimated heat transfer coefficients for different locations on the body as a function of contact pressure varying from 0 to 1 kPa. Generally, the pressure of tight clothing corresponds to 0.5 to 0.8 kPa [43].

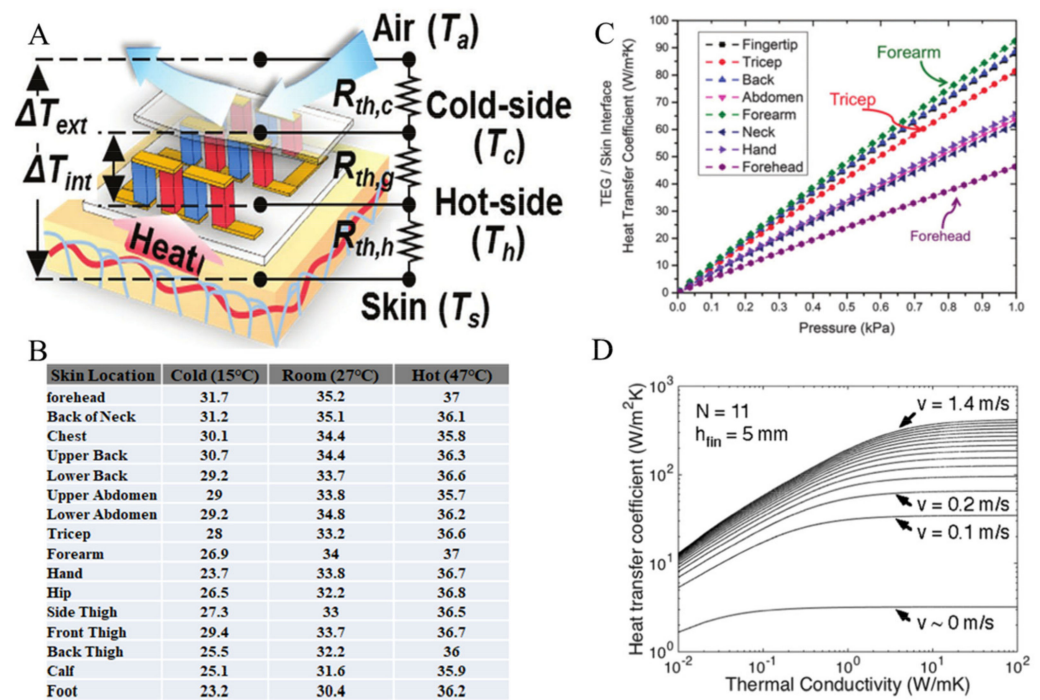


Figure 3. (A) Schematic for the heat transfer model of a wearable thermoelectric generator [37]. (B) Reported human skin temperatures for different points on the body at varying ambient temperatures. (C) Heat transfer coefficient of the TEG/skin interface as a function of pressure for various locations on the body [44]. (D) Heat transfer coefficient of a small heat sink plotted as a function of the thermal conductivity of the heat sink material for different air velocities ranging from almost 0 to 1.4 m/s [44].

Figure 3D shows the calculated heat transfer coefficients for a typical small heat sink consisting of 11 parallel fins, 0.5 mm thick, and 5 mm high. This calculation assumes that the heat sink base area is 1×1 cm and is a function of air velocities and thermal conductivity of the material. The heat transfer coefficient of the heat sink can be used to estimate the air thermal resistance of the interface between the TEG and the air interface [44].

2.3. Different Types of Wearable TEGs Based on Inorganic Bulk Materials

The purpose of WTEGs is to collect more heat for higher output power and be more comfortable for wearing, so the requirements for WTEGs include not only high output power but also flexibility and/or stretchability. The WTEGs are divided into different types and are discussed in detail below.

2.3.1. Rigid Wearable Thermoelectric Generators (r-WTEGs)

Generally, a rigid WTEG consists of a number of pairs of π -type thermoelectric legs connected in series by metal and packaged by two rigid substrates with good thermal conductivity. Rigid-shaped devices are firstly used in commercial products because of their superior heat collection and heat dissipation abilities, which can provide devices with large temperature differences and output power. Seiko Thermic watch (Figure 4A) was the first commercial body-heat-powered wristwatch, which was manufactured in 1998 [45]. The thermal to electrical energy conversion efficiency of this watch was about 0.1%; its open-circuit voltage was 300 mV, and the output power was approximately 25 μ W over 1.5 °C temperature difference across the thermoelectric modules when the watch was worn. It can be equipped with heat sinks according to different application environments. To make the TEG work indoors and on a seated person (without forced air convection), a 38×34 mm heat sink with small pins and a TEG were assembled in a “five-to-seven” design. The “five to seven” design contains 32 thermopiles and a pin heat sink. The

metal protection grid above the TEG protects the heat sink from being touched. The approximate average power generation at daytime of $25\ \mu\text{W}$ corresponds to $20\ \mu\text{W}/\text{cm}^2$, which exceeds solar cells in many indoor situations, especially considering that TEG power is also available at nighttime [46]. In addition, Settaluri et al. added a copper sheet as the high-efficiency heat collector that can fit the human arm and a heat sink to reduce the air thermal resistance for the r-WTEGs, as shown in Figure 4B [47]. The TEG module contains 256 Bi_2Te_3 thermocouples (2 mm thick, $1\ \text{mm}^2$ area) for power generation and two ceramic plates (0.7 mm thick, $10\ \text{cm}^2$ area) for electrical insulation. A 0.1 mm thick flexible copper plate with an area of $14.6 \times 6.4\ \text{cm}$ was employed to make direct contact with the skin and effectively increase heat flow. Infrared images show that the heat sink can increase the temperature gradient for the TEG. Moreover, the heat sink surface can be designed with flat, groove, and checkerboard patterns to increase heat exchange with the air, showing steady-state open-circuit voltages of 85, 94, and 108 mV, and power outputs of 17.6, 21.6, and $28.5\ \mu\text{W}/\text{cm}^2$, respectively. On the other hand, Nozariasbmarz et al. used nanostructured TE materials with a low fill factor (*FF*) module [48]. The fabricated r-WTEGs exhibited about 80% power output enhancement compared to commercial designs, resulting in a high power density of $35\ \mu\text{W}/\text{cm}^2$ (Figure 4C). Conventional bulk TE materials have several weaknesses, including the complexity of processing, heavy-weight, and rigidity, all of which limit their applicability, especially when in contact with curved heat sources. In this regard, flexible thermoelectric generators are promising for wearable applications because their conformability enables effective contact with curved heat sources to maximize heat harvesting.

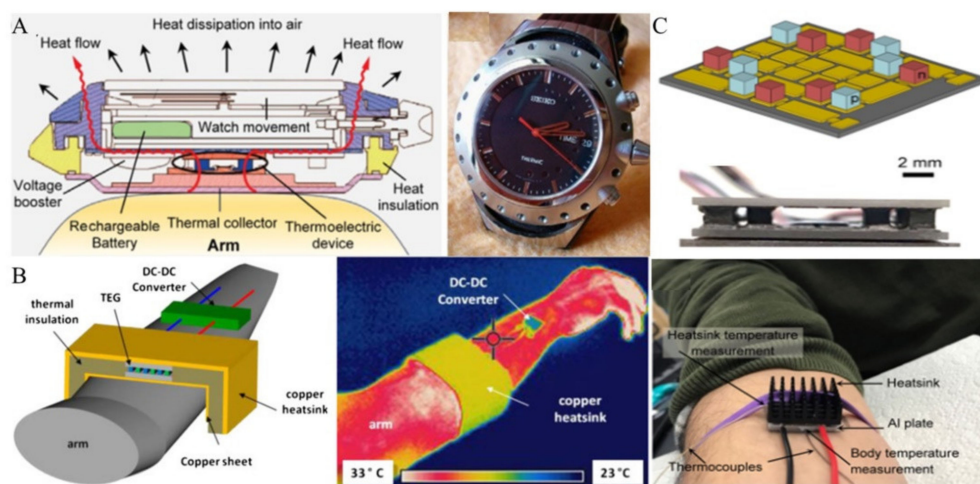


Figure 4. (A) The schematic of the Seiko Thermic watch that could generate about $25\ \mu\text{W}$ from body heat to power the watch [45]. (B) Schematic diagram of a low-profile r-WTEGs and infrared image of copper with a high emissivity coating showing effective cooling using the large surface area available in a wristband [47]. (C) The schematic of a low *FF* TEG module and experimental setup used to measure the TEG module on the human body [48].

2.3.2. Flexible Thermoelectric Generators (FTEG)

Since most human body parts are curved or even dynamic, only a small part of the human body can be used for rigid wearable TEG. In order to obtain body heat from a larger area, flexible wearable devices have been proposed. The FTEG can be divided into two types, one is the non-stretchable FTEG that can be worn on curved surfaces such as human arms, and the other is the stretchable FTEG that can be worn on dynamic surfaces such as joints.

Non-Stretchable Flexible Thermoelectric Generators (ns-FTEGs)

Non-stretchable Flexible Thermoelectric Generators (ns-FTEGs) have achieved great development in recent years due to their wide applicability and high efficiency. A common and simple way to fabricate ns-FTEGs is to connect the TE legs through flexible electrodes, as shown in Figure 5A. The device was fabricated by Yuan et al., using FPCB as the connecting electrode and supporting substrate among TE elements, and considering the multi-objective optimization of power density, material consumption, and power matching with wearable electronic devices [49]. The results show that the ns-FTEGs exhibit excellent flexibility and high output, with power densities of 3.5 and 12.3 $\mu\text{W}/\text{g}$, respectively, under no-wind conditions. In addition, a self-powered wearable bracelet was also fabricated. The strategy was to combine FTEG with a booster, which can be worn on the wrist with an output voltage of 2.8–3.3 V to drive multi-sensory systems, tailor-made intelligent power management, and LCD data displays. The system, which was fully man-powered, could continuously and simultaneously monitor the temperature, humidity, and activity of the human body. ns-FTEGs can be used as a continuous green energy supply for wearable monitoring systems. However, the TE legs of those modules are easily oxidized and fall off the WTEG during application. In order to enhance the reliability of ns-FTEGs during the application, an effective way to encapsulate the TE legs and flexible electrodes together into a flexible encapsulation material is needed. As shown in Figure 5B, Kim et al. used the nickel lift-off method to embed the screen-printed Cu thin film into Polydimethylsiloxane (PDMS) [50]. The design solved the problem of poor adhesion between the Cu electrode and the PDMS, and also prevented the TE legs from being oxidized. The TE module generated an open-circuit output voltage of 2.9 mV and an output power of 3 μW at an ambient temperature of 15 $^{\circ}\text{C}$. Nonetheless, while the encapsulation makes the device more reliable, it inevitably causes a part of the heat to be shunted from the TE legs, thus rendering the device too thin to build a large temperature difference. In 2018, Park et al., proposed a method in which the TE legs were encapsulated by bakelite individually and connected in series by a flexible wire (Figure 5C) [51]. Thus, the TEG possessed good flexibility and reliability. The TE module could generate an output voltage of 8.8 mV and power of 138.67 μW or a power density of 5.60 $\mu\text{W}/\text{cm}^2$ at room temperature. Compared with the two aforementioned structures, the assembly process of this type of TEG is more complicated, leading to difficulty in mass production.



Figure 5. (A) Structural design and fabricated images of ns-FTEGs and FTEGs-powered wearable multi-sensory bracelet [49]. (B) Schematic illustration of the flexibility of the embedded Cu film (Cu foil vs. the screen-printed Cu film) in PDMS and demonstration of band-type flexible TE generator for harvesting thermal energy from human skin at an air temperature of 15 $^{\circ}\text{C}$ (scale bar, 1 cm) [50]. (C) Schematic design and structure of ns-FTEGs encapsulated by bakelite [51].

Stretchable Flexible Thermoelectric Generators (s-FTEGs)

Compared with r-WTEGs and ns-FTEGs, stretchable flexible thermoelectric generators (s-FTEGs) can be applied to complex and even dynamic surfaces to minimize thermal energy loss at the interfaces.

There are various types of stretchable FTEG structures based on organic materials or thin films, but the method of fabrication based on inorganic bulk materials is mainly to use stretchable electrodes to connect thermoelectric legs and encapsulate them with elastic organics. A common material for making stretchable electrodes is liquid metal (LM). As shown in Figure 6A, the device is composed of top and bottom LM-embedded elastomer (LMEEs) layers that act as a heat spreader and form electrical interconnections between the TE legs by LM [52]. The results show that the s-FTEG can perform well after more than 1000 cycles at 30% stretch. At a temperature difference of 10 °C, it could generate an open-circuit voltage of about 60 mV. When the temperature difference is raised to 60 °C, it could generate an open-circuit voltage of about 320 mV and a power density of 0.087 mW/cm². Snake-shaped copper foil is another form of flexible electrode, as shown in Figure 6B [53]. These hot-pressed p-type (Sb₂Te₃) and n-type (Bi₂Te₃) TE legs are interconnected by stretchable snake-shaped copper electrodes and embedded in Ecoflex elastomers. When the s-FTEG is stretched, the flexible snake-shaped copper electrode is elongated to maintain the thermoelectric connection between the TE elements. The results show that its 10 × 10 array device has an internal resistance of 22 Ω, and its output power is about 0.15 mW/cm² at ΔT = 19 K.

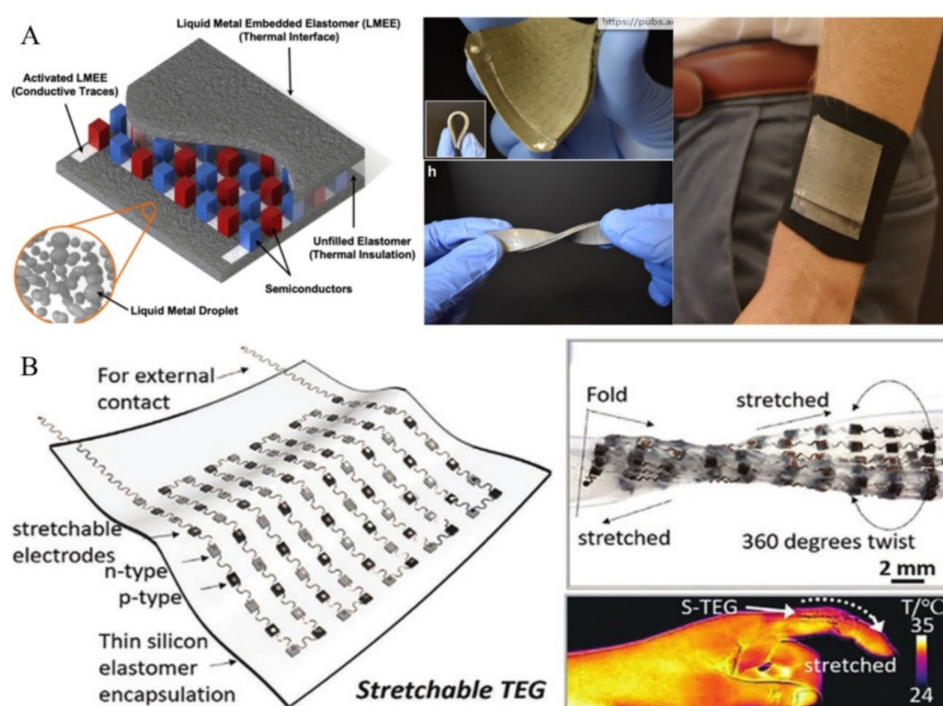


Figure 6. (A) s-FTEGs with stretchable liquid metal electrodes [52]. (B) s-WTEGs with snake-shaped copper electrodes [53].

s-FTEG can be applied to special parts of the human body, such as the joints of limbs, because of its superior flexibility. Among the three wearable TEGs, s-FTEG has the lowest output power but can drive some low-power sensors.

Table 1 shows the performance of the three types of WTEGs. Rigid WTEG has the highest output power, followed by ns-FTEG, and s-FTEG comes at last. Meanwhile, ns-FTEG has attracted the attention of scholars in recent years due to its high output power and its ability to fit most areas of the human body.

Table 1. Performances and features summary for different types of WTEG.

Types of WTEGs	Materials of TE Legs	ZT or Efficiency	Encapsulation	Electrode	Ambient Temperature	Heat Sink	Power Density ($\mu\text{W}/\text{cm}^2$)	Ref.
r-WTEG	Bismuth Telluride	0.8	PDMS/Alumina	Copper	18.3 °C	Heat spreader	6	[54]
r-WTEG	Commercial Bi_2Te_3	/	Alumina	Copper	22 °C	Plate fin heat sink	20	[46]
r-WTEG	Commercial Bi_2Te_3	/	Ceramic	Copper	23 °C	Plate fin heat sink	28.5	[47]
r-WTEG	Bi_2Te_3	0.14%	AlN	Copper	17 °C	Plate fin heat sink	35	[48]
r-WTEG	Bi_2Te_3	/	AlN	Copper	25 °C	Heat spreader	44	[55]
ns-FTEG	Commercial Bi_2Te_3	/	PDMS	FPC	13 °C	No	0.084	[56]
ns-FTEG	Bi_2Te_3 (Glass fabric)	/	PDMS	Copper	15 °C	No	0.75	[50]
ns-FTEG	Commercial Bi_2Te_3	/	No	FPC	19 °C	No	0.4	[57]
ns-FTEG	Commercial Bi_2Te_3	/	PDMS	FPC	25 °C	No	0.526	[58]
ns-FTEG	Commercial Bi_2Te_3	/	Polymer	Copper	25 °C	No	2.28	[59]
ns-FTEG	Commercial Bi_2Te_3	0.35	PDMS	LM	5 °C	No	2.5	[60]
ns-FTEG	Commercial Bi_2Te_3	0.85	No	FPC	13 °C	No	3.5	[49]
ns-FTEG	Commercial Bi_2Te_3	0.71	PDMS	Copper	24 °C	No	4.5	[61]
ns-FTEG	Commercial Bi_2Te_3	/	PDMS	LM	24 °C	No	5.2	[62]
ns-FTEG	Commercial Bi_2Te_3	/	Aerogel/PDMS	LM	24 °C	No	5.4	[63]
ns-FTEG	Commercial Bi_2Te_3	/	MF	Copper	24 °C	Heat spreader	7	[64]
ns-FTEG	Bi_2Te_3	/	Bakelite	Copper	20 °C	Plate fin heat sink	1.6	[65]
ns-FTEG	Bi_2Te_3	/	Bakelite	Copper	24 °C	Flexible heat sink	4.78	[51]
ns-FTEG	Bi_2Te_3	/	Bakelite	Copper	24 °C	Flexible heat sink	5.6	[66]
ns-FTEG	Bi_2Te_3	/	Bakelite	Copper	24 °C	Plate fin heat sink	5.6	[67]
ns-FTEG	Bi_2Te_3	0.75	Fabric	Copper	24 °C	Air velocity: 0.2m/s	6.3	[68]
ns-FTEG	Bi_2Te_3	/	No	Copper	24 °C	Plate fin heat sink	8	[69]
ns-FTEG	Bi_2Te_3	/	PDMS	LM&Copper	24 °C	Hydrogels	8.3	[65]
ns-FTEG	Commercial Bi_2Te_3	0.75	Porous PDMS	Copper	24 °C	SAP heat sink	9.7	[70]
ns-FTEG	Commercial Bi_2Te_3	0.68	Polymer	Copper	24 °C	SAP heat sink	13	[71]
ns-FTEG	Bi_2Te_3	/	No	FPC	24 °C	Radiant cooling	12.5	[72]
ns-FTEG	$\text{Mg}_3\text{Bi}_2/\text{Bi}_2\text{Te}_3$	/	Porous PU	Copper	16 °C	Air velocity: 1.1m/s	20.6	[73]
ns-FTEG	Commercial Bi_2Te_3	0.64	Polymer	Copper	13 °C	PCM heat sink	20	[74]
s-FTEG	Bi_2Te_3 (PEDOT:PSS)	/	PDMS	Copper	$\Delta T=33\text{K}$	No	0.87	[53]
s-FTEG	Bi_2Te_3	/	Elastic fabric	Polyester Fiber	$\Delta T=33\text{K}$	No	1	[75]
s-FTEG	Commercial Bi_2Te_3	/	PDMS	LM	$\Delta T=10\text{K}$	No	4	[52]
s-FTEG	Bi_2Te_3	/	PDMS/Ag-Ni	AgNW	10 °C	No	6.97	[76]

LM: liquid metal. SAP: absorbent polymer. MF: Melamine foam. PU: Polyurethane. AgNW: Silver nanowires.

3. Optimization of Wearable Thermoelectric Generators

3.1. Materials for Wearable Thermoelectric Generators

Thermoelectric legs are the basic elements of thermoelectric power generation devices and thermoelectric heating and cooling devices. The improvement of their performance plays an indispensable role in the performance of the entire thermoelectric device. At present, the research of inorganic thermoelectric materials mainly focuses on metals and semiconductor alloys. There are three main categories of thermoelectric materials, namely high-temperature thermoelectric materials, such as silicon-germanium, intermediate-temperature thermoelectric materials, such as lead-telluride, and room-temperature thermoelectric materials, such as bismuth-telluride [77–79]. In general, wearable thermoelectric generators work around room temperature, and inorganic bulk thermoelectric materials with good thermoelectric performance at room temperature are discussed below.

3.1.1. Bismuth Telluride Material

Bi_2Te_3 is the best candidate for thermoelectric materials working at around room temperature. It was firstly reported in the 1950s. Bi_2Te_3 is a narrow gap-layered semiconductor material with a bandgap energy of about 0.15 eV; its crystalline structure belongs to the rhombohedral crystal system and space group $R\bar{3}m$ [55,80–82]. Bi_2Te_3 crystals have a layered structure, consisting of one kind of Bi site and two kinds of Te site, which form a five-layered crystal structure. Two adjacent Te layers are bound by van der Waals force, which causes easy cleavage [83].

In practical applications, the solid solutions of Bi_2Te_3 and Sb_2Te_3 are commonly used to prepare p-type materials $(\text{Bi}_x\text{Sb}_{1-x})_2\text{Te}_3$. The regulation of the hole carrier of Bi_2Te_3 can be achieved by combining a Sb_2Te_3 solid solution with Bi_2Te_3 , which also introduces a large number of point defects to significantly reduce the lattice thermal conductivity of the material. The n-type $\text{Bi}_2\text{Te}_{3-x}\text{Se}_x$ can be obtained from solid solutions of Bi_2Te_3 and Bi_2Se_3 . Both components are appropriate for body heat harvesting thanks to their high thermoelectric performance [38].

For half a century, many methods have been attempted to improve the thermoelectric properties of Bi_2Te_3 , including the synthesis of low-dimensional nanomaterials, the optimization of material composition through doping, and the development of novel preparation processes [84]. Typically, the zone melting method is a traditional method for preparing Bi_2Te_3 , through which samples with a ZT value of about 1 can be obtained. However, because Bi_2Te_3 is prone to cleavage and belongs to the direction of crystal growth, it is fragile and possesses poor mechanical properties. Hence it is difficult to process and not suitable for wearable devices. Therefore, to overcome the mechanical and thermoelectric challenges, numerous studies have been carried out on the preparation of dense polycrystalline bulk material by powder sintering process, including hot pressing and spark plasma sintering. Zheng et al., prepared a p-type $\text{Bi}_{0.5}\text{Sb}_{1.5}\text{Te}_3$ compound by combining melt spinning with SPS. The bending strength and compressive strength of this sample were 5 times and 3 times higher than that of the zone melting one, respectively, and the ZT value also reached a maximum value of 1.22 at 340 K [85]. In addition to the sintering process, the introduction of nanostructures also greatly improves the thermoelectric properties of materials. Through effectively scattering phonons by decreasing grain size, introducing point defects, and dislocation arrays to the grain boundary, the lattice thermal conductivity can reduce rapidly, which improves the thermoelectric properties [22]. For bulk materials, ball milling and melt spinning are the most common ways of making grain size nanoscale. Kim et al. successfully prepared $\text{Bi}_{0.5}\text{Sb}_{1.5}\text{Te}_3$ by using melt spinning together with Te composite, reducing the lattice thermal conductivity to $0.33 \text{ Wm}^{-1}\text{K}^{-1}$ and obtaining the highest ZT value of 1.86 at 320 K [86]. Poudel et al. prepared p-type $\text{Bi}_x\text{Sb}_{2-x}\text{Te}_3$ nanocomposites with ZT values of 1.4 at 100 °C by ball milling combined with hot-pressing [87]. Like the introduction of nanostructures, modulation doping is still an important method to improve the thermoelectric performance of Bi_2Te_3 . For example, the thick graphene nanoplatelets (GNPs) at the grain boundaries of Bi_2Te_3 polycrystal can boost the ZT value to 1.5, which increases the device output power by 35% [82]. Apart from the above two methods, there are several novel processes employed to achieve the control of defects and nanostructures. For instance, Nozariasbmarz et al. investigated the fact that combining microwave processing, glass inclusions, and annealing could enhance the ZT value of p-type $(\text{Bi}_x\text{Sb}_{1-x})_2\text{Te}_3$ to 1.2 at room temperature by introducing defects, which promoted a significant reduction in thermal conductivity [88].

In recent years, low-dimensional nanoscale-related research has further refined the thermoelectric properties of materials. In 2022, Chen et al., reported a flexible film of n-type Bi_2Te_3 /single-walled carbon nanotube (SWCNT) hybrids with a cement-rebar nanoarchitecture constructed by a new solution-processed method. Benefiting from the novel structure, an extremely low thermal conductivity of $\sim 0.33 \text{ Wm}^{-1}\text{K}^{-1}$ was realized at room temperature. Furthermore, the TE performance of this film is independent of mechanical bending, which makes it applicable to practical devices [28]. Different from traditional

alloys, superlattice material is a kind of thermoelectric material that uses acoustic mismatch between superlattice components to reduce lattice thermal conductivity and improve the ZT value. The ZT value of the superlattice material ($\text{Bi}_2\text{Te}_3/\text{Sb}_2\text{Te}_3$) can reach 2.4 at 300 K [89]. Compared with the bulk material, the superlattice film greatly improves the material properties of Bi_2Te_3 . If this type of thin-film material possesses excellent flexibility and lower manufacturing costs, it will be more suitable for wearable devices.

3.1.2. Other Room Temperature TE Materials

Bi_2Te_3 -based thermoelectric materials have been widely used in the industry due to their excellent performance and decent price. However, tellurium compounds are considered mildly toxic and have poor mechanical properties. At present, the TE materials with better performance at room temperature are Ag_2Se [90], MgAgSb [91–93], SnSe [94–97], Ag_2Te [98–100], PbTe [101], etc. PbTe and Ag_2Te are tellurides, which we will not discuss. It is worth noting that the MgAgSb -based material is also a non-toxic and better-performing material with good mechanical properties that is expected to replace Bi_2Te_3 . There are three different crystal structures in MgAgSb : a half-Heusler γ phase at high temperatures (630–700 K), a Cu_2Sb -related β phase at about 560–630 K, and a tetragonal structure α phase with $a = 9.1761 \text{ \AA}$ and $c = 12.6960 \text{ \AA}$ at low temperatures (under 560 K) [F4]. MgAgSb can improve its TE performance by adjusting the percentage of Ag and Sb. Zhao et al. used ball milling and obtained an alloy with a ZT value of 0.7 at room temperature [102]. With the addition of multi-walled carbon nanotubes (MWCNTs), the electrical conductivity of the MgAgSb increases dramatically. This is because the addition of MWCNTs improves both phonon scattering and electrical transportation. At room temperature, the ZT of $\text{MgAg}_{0.97}\text{Sb}_{0.99}$ with 0.1 wt% MWCNTs is 0.83 [103]. Furthermore, the performance of MgAgSb can be optimized by Zn-doping and heat-treating. Zheng et al. obtained a method for preparing MgAgSb with excellent properties. The average ZT is about 1.3 in the range from 323 to 548 K in the sample $\text{Mg}_{0.97}\text{Zn}_{0.03}\text{Ag}_{0.9}\text{Sb}_{0.95}$ with heat-treating for 10 days, which is one of the highest values among all reported p-type MgAgSb -based thermoelectric materials. Tin selenide (SnSe) is one of the most efficient thermoelectric materials because it has low thermal conductivity as well as reasonable electrical conductivity. It has two stable phases: low-temperature α - SnSe ($T < \sim 800 \text{ K}$) and high-temperature β - SnSe ($\sim 800 \text{ K} < T < 1134 \text{ K}$). The mechanical properties of polycrystalline SnSe are comparable to other advanced thermoelectric materials [95]. For low-temperature α - SnSe , Zhao et al. obtained a high ZT of about 1.34, ranging from 0.7 to 2.0 at 300 to 773 K, realized in hole-doped tin selenide (SnSe) crystals [97]. As Su et al. reported, they found an average ZT of about 1.7 at 300 to 773 K in chlorine-doped and lead-alloyed tin selenide crystals by phonon-electron decoupling [96]. For high temperature use, Zhou et al., used hole-doped SnSe polycrystalline samples and with tin oxides, removed an exhibit of ZT of roughly 3.1 at 783 K. The key to performance enhancement is to remove the deleterious, thermally conductive oxides from the surface of SnSe grains [94]. Ag_2Se -based TE materials are also well-studied. They are less toxic and can be prepared by costless synthetic methods. Silver and selenium powder can be mixed at room temperature, but the price of silver powder is a little high. It has been reported that the ZT value of Ag_2Se obtained by doping carbon nanotubes with 0.5 wt% can reach 0.88 [104]. Day et al., calculated and predicted Ag_2Se with a ZT around 1.0 using a single parabolic band model [105], and it was experimentally proven to show $ZT \sim 1.0$ near room temperature through optimizing the composition and nanostructure control [106]. With the development of Ag_2Se -based thermoelectric materials and the requirement of removing Te from industrial materials, Ag_2Se is expected to replace Bi_2Te_3 -based materials as a room temperature thermoelectric material. Nanostructure TE materials are promising in WTEG and other fields. It has a larger Seebeck coefficient, and a large number of nanometer features in nanomaterials can effectively scatter phonons and reduce thermal conductivity, which could increase the ZT of the TE materials. The progress of nanostructured bismuth telluride has also stimulated the development of other thermoelectric materials in the nanometer direction to some extent. Jiang et al. have tried to

obtain a high-performance Ag_2Se film with a power density of 22.0 W/m^2 . It was realized by the synthesis of multi-sized Ag_2Se nanostructures [107]. In addition, nanostructured monoclinic Cu_2Se with a low carrier concentration has been synthesized by a wet mechanical alloying process combined with spark plasma sintering. It has obtained a ZT of 0.72 at 380 K by Chen et al. [108].

3.2. Device Design Optimization for Wearable Thermoelectric Generators

3.2.1. Geometric Parameters

The performance of a WTEG is determined by its temperature difference and the heat flow through the TE legs, while the temperature difference of TEG is mainly determined by its thermal resistance in a given ambient condition. The thermal resistance of TEG can be increased by reducing the fill factor, i.e., reducing the number of TE legs. In addition, increasing the aspect ratio of the legs and/or reducing the thermal conductivity of the legs can also play the same role [44,109,110], but this also affects the amount of heat flowing through the TE leg. Wherefore the optimal matching of several parameters must be considered in improving the output of WTEG. Leonov et al. reported a thermal resistance-matching mechanism to optimize the performance of WTEG and the thermal resistance of TEG should satisfy Equation (14) [111]:

$$R_{th,g,optimal} = \frac{R_{th,F}(R_{th,h} + R_{th,c})}{2(R_{th,h} + R_{th,c}) + R_{th,F}} \quad (14)$$

where $R_{th,F}$ is the parallel parasitic thermal resistance in a TEG upon the imaginary removal of the TE material, $R_{th,h}$ is the thermal resistance between the body core and the surface of the skin, and $R_{th,c}$ is the thermal resistance of the ambient air. However, the study by Leonov et al., cannot directly predict the output of the TEG from the specific geometric parameters of the TE legs.

In order to express the influence of the geometric parameters of WTEG more intuitively and multi-dimensionally, Lee et al. analyzed the influence of the length, width, and FF of the thermoelectric leg on the output performance of a device under different convection conditions by a numerical analysis method and the results are summarized in Figure 7A [37]. The results clearly show that the length and FF of the TE legs affect the power output of the WTEG, and the width and FF affect the voltage output of the WTEG. In 2020, Zhu et al., proposed a simplified system considering external thermal resistance, output power, and voltage matching [112]. It takes the engineering length (L^*), that is, the ratio of L and FF , as the key parameter for determining the power density of the device and the aspect ratio ($r = L/A$) as the key parameter for the voltage density. The optimizations above are all based on numerical analysis, which cannot be applied for lateral heat transfer. This type of method is reliable for rigid TEG or in the case of good heat transfer. However, the results are not reliable for most flexible TEGs due to their poor heat transfer. Zhu and Peng et al. introduced the influence of the width of the thermoelectric legs on the output power of the flexible TEG using finite element analysis [64]. They proposed that in the case of poor heat transfer, tall and thin thermoelectric legs are more suitable than thick legs. By contrast, in the case of poor heat transfer, the influence of the width of the thermoelectric leg on the thermoelectric power output can be ignored (Figure 7B).

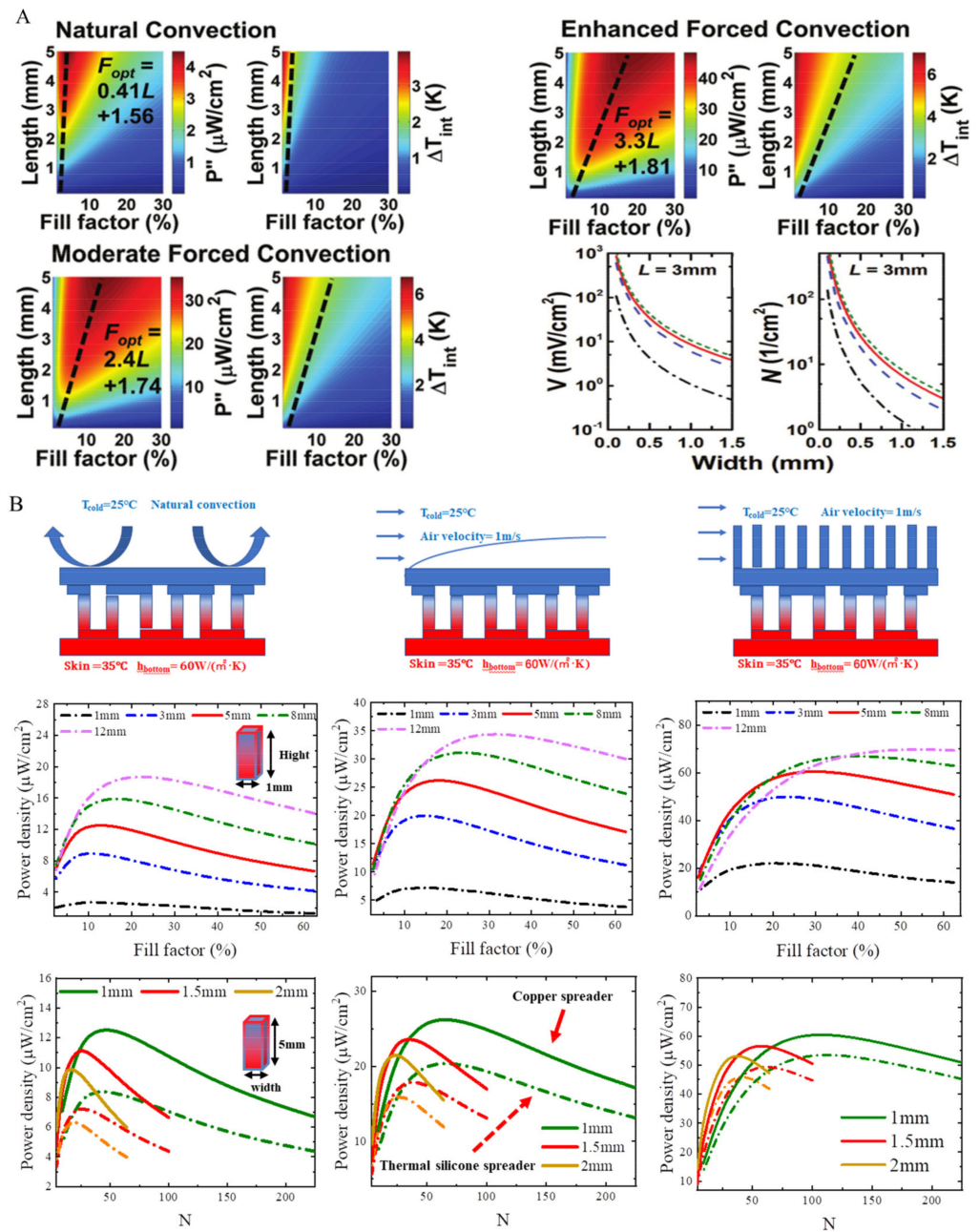


Figure 7. (A) Results of TE geometric parameters obtained by numerical analysis [37]. (B) Results of TE geometric parameters obtained by Finite Element Simulation [64].

3.2.2. Heat Sink

Based on the thermoelectric principle, the output power of WTEG is proportional to the square of the temperature difference (ΔT), so the optimization of temperature difference must be considered [113,114]. The temperature difference depends on the thermal design of the WTEG system, and adding a heat sink to the WTEG is an effective method of increasing the temperature gradient. It goes without saying that, for the WTEG system, not only temperature difference but also flexibility is required for the heat sink. Various designs of heat sinks for WTEG are discussed in detail below.

Figure 8A shows the temperature distribution in a typical wearable TEG system at room temperature and in a cold environment. The results show that more than 40% of the heat is lost at the interface between the TEG and the air, while 20–30% of the heat is lost at the interface between the TEG and the human body, and only less than 30% of the heat can

be used for power generation in the TEG [44]. The contact thermal resistance between the skin and TEG can only be optimized slightly, because it is affected by pressure and skin roughness. Although it can be reduced by increasing the pressure, doing so will make it less comfortable to wear. The heat sink is an effective means to reduce the thermal resistance of the TEG and air interface and has accumulated attention in recent years. For example, Park et al. added a plate fin heat sink to each pair of π -type thermocouples in the chain f-TEG to obtain a large temperature difference while maintaining its flexibility (Figure 8B) [67]. When worn on the wrist and during the “walking” condition, it successfully generated an open-circuit voltage of 12.1 mV with a power output density of $6.97 \mu\text{W}/\text{cm}^2$. However, high fin heat sinks can compromise wearing comfort. Hyland et al., added and optimized a Cu heat spreader with an area of 16 cm^2 and a thickness of $250 \mu\text{m}$ on the cold side of the rigid WTEG (Figure 8C) [54]. The results show that the device equipped with the heat spreader successfully generated a power output density of $6 \mu\text{W}/\text{cm}^2$ when the ambient temperature was $18.3 \text{ }^\circ\text{C}$. A spreader effectively improves the lateral heat transfer but has limited ability to transfer heat to the external environment. In order to enhance the external heat transfer, Kim et al., fabricated a water-storage heat sink based on superabsorbent polymer (SAP) material for FTEG [71]. The thermoelectric power density was increased to $13 \mu\text{W}/\text{cm}^2$ and could be maintained for 22 h through the strategy of water evaporation, which took away the heat from the cold side of the TEG (Figure 8D). Unlike the evaporation of water for the heat sink, which requires continuous water replenishment, Lee et al. used the heat sink to enhance the output of TEG based on solid-liquid phase change material (octadecane), as shown in Figure 8E [74]. While the flexible heat sinks can be reused after solidification at room temperature, the results show that the power generated by the flexible TEG remained at $20 \mu\text{W}/\text{cm}^2$ only for 33 min. Phase change materials based on octadecane have not been able to satisfy the long-term energy supply of electronic systems. In the future, high phase change latent heat materials will also be the way to improve TEG output. Compared with other thick and heavy heat sinks, radiative cooling can be realized by thin films to enhance the flexibility of TEGs, which has attracted the extensive attention of scholars in recent years. Khan et al. proposed a TEG integrated with a flexible, micrometer-thin poly (vinylidene fluoride-co-hexafluoropropylene) radiative cooling heat sink (Figure 8F) [65]. The radiative cooling heat sink can radiate heat to the cosmic space through the atmospheric window, and the fabricated TEG achieves a power density of $12.48 \mu\text{W}/\text{cm}^2$ (outdoors). This TEG module is not only small but also provides high output power compared to TEGs with plate fin heat sinks.

3.2.3. Encapsulation Material

The package is to stabilize and protect the π -type thermoelectric structure. For different TEG applications, encapsulation has various requirements for thermal conductivity, oxidation resistance, and heat insulation. Here, we divide the packages into two categories: substrates for encapsulating electrodes and filler material for encapsulating thermoelectric legs. Different types of encapsulations are discussed in detail in the sections below.

Substrate

The function of the substrate for rigid WTEG is to fix and enhance the lateral heat transfer, and its materials are generally aluminum oxide and aluminum nitride with high hardness and high thermal conductivity and insulation. However, the substrate material of flexible or stretched WTEG is mainly elastomer (PDMS), which can stabilize and protect the electrode from oxidation. Because of its low thermal conductivity, PDMS resists the lateral heat transfer between the hot and cold ends of WTEG, so the modification to make PDMS with higher thermal conductivity has become a hot spot in recent years. For example, Hong et al. doped AlN in Ecoflex to enhance the thermal conductivity [61]. This successfully increased the thermal conductivity of Ecoflex from 0.16 to $0.76 \text{ W}/\text{mK}$. The thermoelectric device with an area of $5 \times 5 \text{ cm}$ is composed of 72 pairs of thermocouples, which can not only be used to manage human body temperature but also generate a power density of

$4.5 \mu\text{W}/\text{cm}^2$ at room temperature. Coincidentally, Sargolzaeiaval et al. also added eutectic gallium indium (EGaIn) to PDMS to improve the thermal conductivity of the substrate for WTEG based on liquid metal electrodes (Figure 9). Worn on the wrist, it achieved a power density of $5.2 \mu\text{W}/\text{cm}^2$ under natural convection and over $30 \mu\text{W}/\text{cm}^2$ at an air velocity of 1.2 m/s [62].

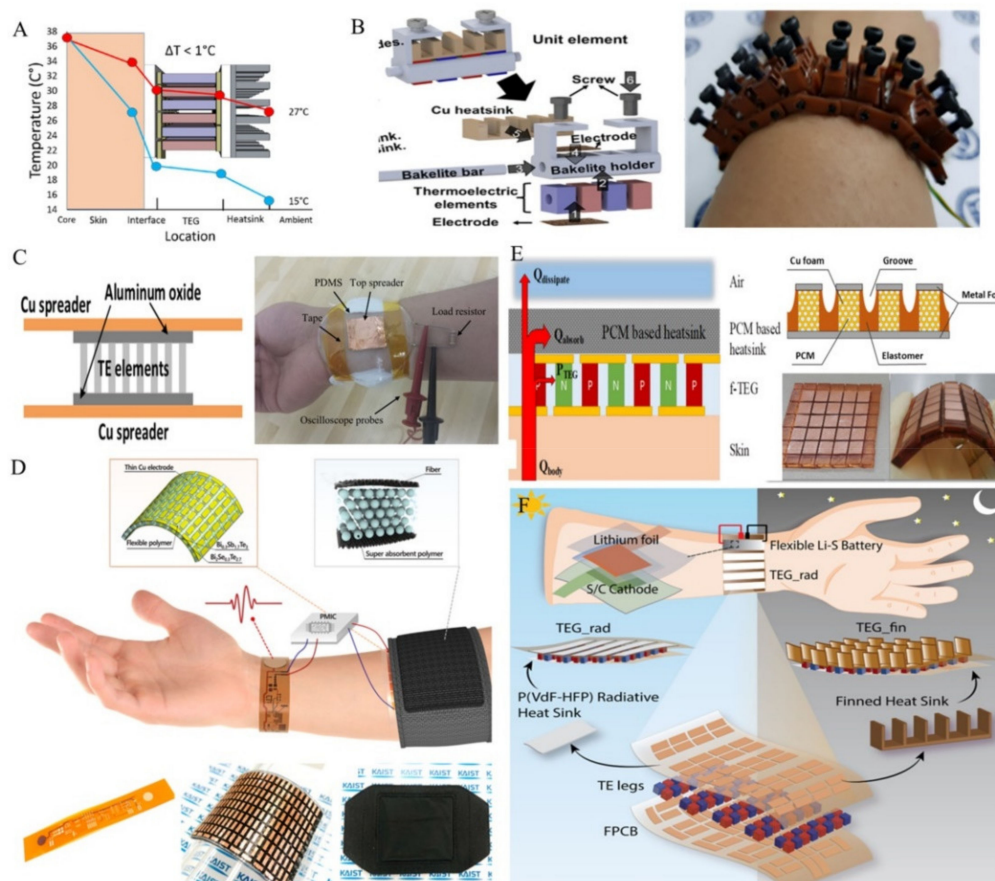


Figure 8. (A) Temperature difference from core body temperature to the ambient air [44]. (B) Schematic structure of FTEG with a copper heat sink and the fabricated device worn on the wrist [67]. (C) Schematic of the r-WTEG with a heat spreader and the experimental setup of the TEG on the wrist [54]. (D) Schematic of the FTEG with a flexible heat sink base on SAP [71] (E) with a flexible PCM heat sink [74] and (F) with a radiative cooling heat sink [72].

Filler Material

In contrast to the substrate, the fill material requires thermal insulation to reduce thermal shunting through the TE legs. Figure 10A shows the results of PDMS and melamine foam (MF) simulated by Zhu et al. [64]. The low thermal conductivity of MF can not only increase the output power but also reduce the fill factor and enhance the flexibility of the device. Figure 10B shows a schematic diagram of its optimized strategy using low thermal conductivity MF as the filler material. A power density of $7 \mu\text{W}/\text{cm}^2$ was achieved in a natural environment. Using a strategy similar to that adopted by Zhu for low thermal conductivity MF, Jung et al. prepared porous PDMS (Figure 10C) [70]. The power density reached $9.7 \mu\text{W}/\text{cm}^2$ when equipped with a SAP based heat sink. Obviously, the method of low-cost and high-efficiency filler material fabrication will continue to be a hot issue in the future.

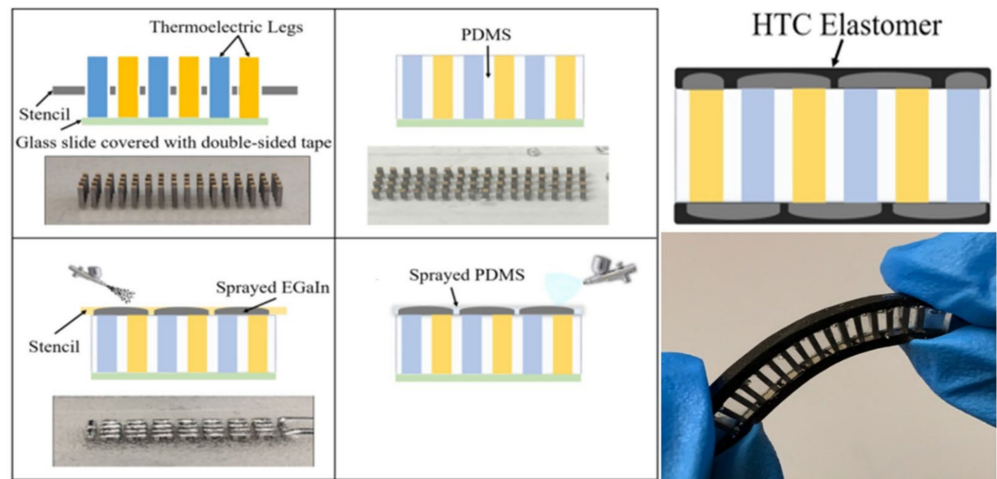


Figure 9. Schematic of the FTEG with flexible high thermal-conductivity substrates based on EGeIn/PDMS [62].

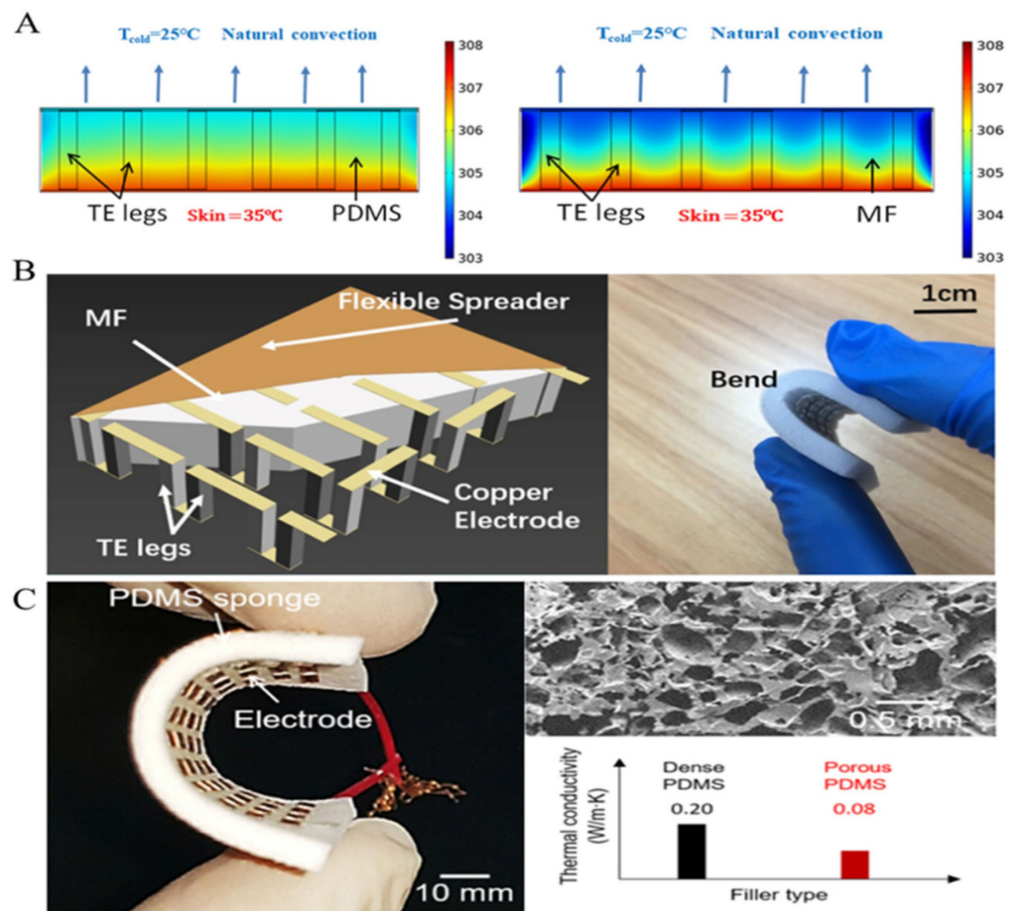


Figure 10. (A) The internal temperature distributions of the TEG filled with PDMS and MF [64]. (B) Schematic of the WTEG filled with MF [64]. (C) Schematic of the WTEG filled with porous and thermal conductivity of PDMS and porous PDMS [70].

3.2.4. Fabricating Process of Thermoelectric Modules

At present, the manufacturing technology based on rigid thermoelectric devices for refrigeration has matured. A low-cost and high-efficiency fabrication process for the commercialization of flexible wearable thermoelectric generators is the key. In 2016, Kim et al. reported FTEGs produced by screen printing technique (SPT) and laser multi-scanning (LMS) lift-off process. Screen-printed TEGs were fabricated on $\text{SiO}_2/\text{a-Si}/\text{quartz}$ substrates by the SPT process, and then rigid quartz substrates were completely separated from pristine TEGs (a-Si) by the LMS process [115]. The FTEG fabricated by this technique exhibits high flexibility (no significant change in device performance after 8000 repeated bending cycles) and excellent output performance ($4.78 \text{ mW}/\text{cm}^2$ and $20.8 \text{ mW}/\text{g}$ at $\Delta T = 25 \text{ }^\circ\text{C}$). However, the fabrication process is complicated. In 2018, Shi et al., proposed a low-cost and efficient FTEG fabrication method based on the commercialized flexible printed circuit (FPC), as shown in Figure 11A [58]. It was first arranged and fixed on the TE legs through the sieve tray and then welded onto the customized FPC. This semi-automatic assembly method is simple and low-cost, but the assembly and welding of electrodes are still complicated and inefficient. Zhu et al. simplified this step through etching techniques [64]. They first printed the circuit on transfer paper and then transferred it to copper foil with PI on the back, and finally etched the electrodes. As to the assembling technology of s-FTEG, Li et al. proposed a highly automated fabrication process by doping silver-nickel (Ag-Ni) particles into PDMS to improve the thermal conductivity of the substrate, as shown in Figure 11B [76]. Ag-Ni particles were first mixed with PDMS, and then silver nanowires (Ag-NWs) were printed as soft electrodes onto the mixture through a mask. Afterward, the mixture of PDMS and Ag-Ni particles was magnetically aligned along the direction of the legs to facilitate heat transfer from the skin to the legs. Next, 220 couples of Bi_2Te_3 -based TE legs were automatically arranged onto the Ag-NW electrodes via vacuum suction nozzles, and then the gaps between them were filled with PDMS. The electrodes of the upper substrate are prepared in the same way and mounted on top of the device. The highly automated fabrication process greatly improves fabrication efficiency. The results show that when the flexible TEG with an area of $39 \times 43 \text{ mm}^2$ is worn on the wrist, the highest power density generated under a $10 \text{ }^\circ\text{C}$ temperature gradient is $6.96 \text{ } \mu\text{W}/\text{cm}^2$.

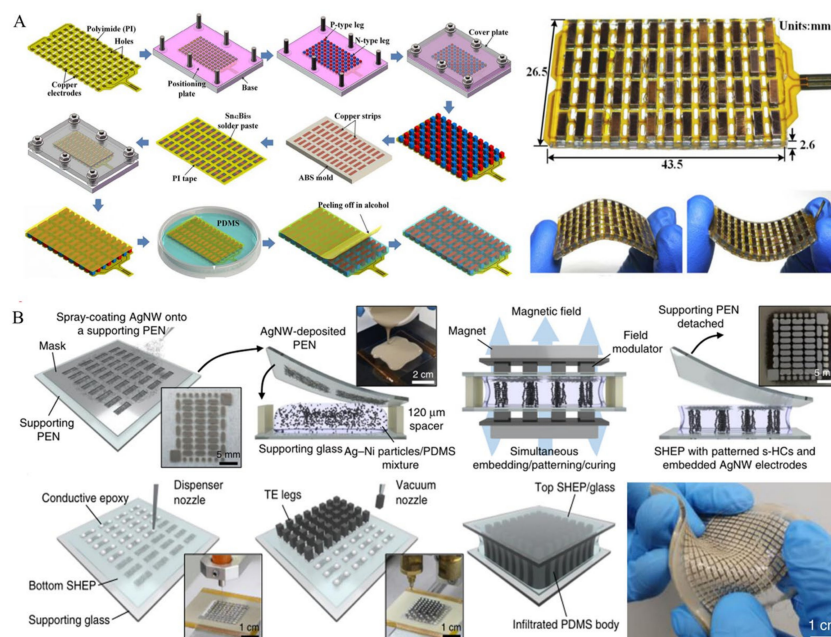


Figure 11. (A) Semi-automatic fabrication process for the wearable TEG based on FPCB and the fabricated device [58]. (B) Highly automated fabrication process for the wearable TEG based on AgNW electrode and the fabricated device [76].

4. Thermoelectric and Wearable Applications

In recent years, major breakthroughs have been witnessed in low-temperature thermoelectric materials in terms of performance and flexibility. More efficient, lightweight, and safe thermoelectric devices have been reported one after another. Wearable devices have great potential applications in healthcare, environmental detection, and other fields. This paper summarizes the application and market of thermoelectric wearable devices in the following two aspects.

4.1. Market Research for Wearable Thermoelectric

The global thermoelectric generator market was valued at 472.5 million USD in 2020 and is projected to reach 1443.3 million USD by 2030, growing at a compound annual growth rate (CAGR) of 11.8% from 2021 to 2030. The thermoelectric generators market is segmented into low power (<10 W), medium power (10 W–1 kW), and high power (>1 kW) based on wattage. The power produced by thermoelectric generators is highly dependent upon the temperature applied to their plates. The low power (<10 W) segment of the thermoelectric generators market is projected to grow at the highest CAGR during the forecast period, with the increasing use of wearables and handheld consumer electronic devices being the major. In the context of the global COVID-19 pandemic, wearables devices are rapidly moving into the preventative care, diagnostics, and urgent care segment with an anticipated market of 9.3 B USD by 2024, driving improvement of the WTEG market [116].

4.1.1. Biomedical Devices

The demand for autonomous monitoring and diagnosis is large in the healthcare industry since the increasing healthcare costs and the rapid aging of the global population in developed countries. By 2030, for example, nearly 25% percent of US residents are expected to be aged 65 or older. Among them, heart rate, pulse, and other health indicators need to be as continuous as possible, and TE materials can provide energy for wearable devices to avoid the potential danger of battery replacement to the greatest extent. In some relatively simple applications proposed earlier, it is confirmed that this wearable detection device based on WTEG can be realized and applied in the medical field. Tom et al. used a small watch-type thermoelectric generator to build a wireless pulse oxymeter powered by body heat [117]. The system, shown in Figure 12A, is an integration of WTEG and wireless sensing, has an output of about 30 μ W per square centimeter when the watch is close to the skin, and the watch is large enough to provide a steady stream of power to the sensor. However, this kind of watch-type thermoelectric device has poor flexibility and should develop in the direction of higher comfort and flexibility under the premise of meeting the power supply demand. In Figure 12B, Kim et al. printed the conventional thermoelectric power generation and regeneration circuit in the flexible PCB, giving the device higher flexibility and adding the flexible heat sink to enable sufficient temperature difference, successfully establishing the self-powered wearable ECG system at the arm site [71]. This flexible design ensures the energy of the ECG system while greatly improving the comfort experience. With the continuous improvement of the flexibility and efficiency of thermoelectric wearables, more and more previously undesirable applications have been reported, in addition to routine tests, such as blood pressure, pulse and heartbeat. A self-powered hearing aid based on thermoelectric power generation devices was proposed and designed by Ekuakille et al. [118]. As shown in Figure 12C, the hearing aid is mainly composed of an amplifier circuit, which has extremely low power consumption. In daily life, the power supply can be achieved entirely by the body heat-driven flexible thermoelectric device, a design that truly makes the external hearing aid an “artificial ear”.

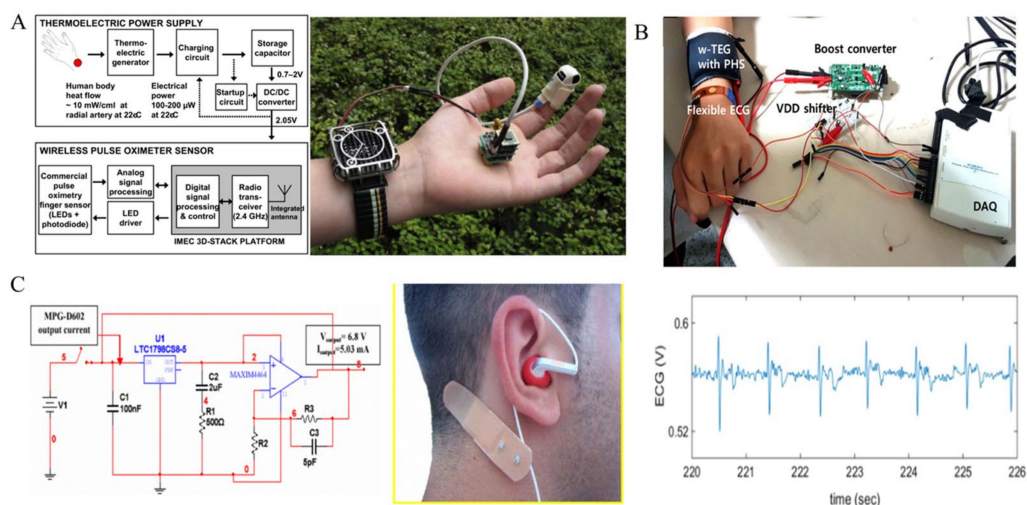


Figure 12. (A) Watch-type thermoelectric and oximeter [117]. (B) Flexible thermoelectric ECG detector [71]. (C) Thermal and power hearing aid [118].

4.1.2. Human Activity Monitoring Device

Flexible thermoelectric systems that monitor human motion states can provide fully continuous detection in clinical diagnosis, behavioral analysis, and information communication. Shi et al. developed a wearable thermoelectric system that can monitor the motion state of a person in real-time [58]. The system is powered by the body heat of the wrist and provides continuous detection based on inertial and strain sensors. It can determine the wearer's current movement state only through the feedback waveform. Although it can assess significant state changes, such as running, jumping, and walking, it is subtle, such as speed discrimination (Figure 13A). More precise sensors are helpful for detecting movement status. Yang et al., proposed a hand state detection device self-powered by WTEG [53]. The system uses the stress tensile sensor to detect more sensitive factors, and subtle changes in hand movements can be seen in Figure 13B. This wearable application based on a highly sensitive stretch sensor is also widely used in laryngeal language discrimination and ocular visual sensing, but motor state recognition devices in which more flexible thermoelectric systems collect energy from the dynamic surface of the human skin have not been reported.

4.1.3. Environmental Monitoring Device

Signals from the surrounding environment (such as ultraviolet light, air composition, temperature) are also important compared with health care. Wearable devices can help the wearer visualize unknown signals from the environment and reduce/avoid health hazards from the environment, and even predict potential hazards. The focus is on people in hazardous operations. Lee et al. designed a wearable temperature measurement glove driven by an FTEG. It can accurately measure the temperature of touching objects with a temperature-sensitive sensor and warn users with LEDs to avoid burns caused by touching unknown objects [76]. In addition to the above temperature detection thermoelectric gloves, more practical, lighter, and more fully functional hand wearables have been reported (Figure 14A). In 2020, Yuan et al., introduced a TE system that can help the wearer perceive more external information [119]. The system has the functions of monitoring temperature, humidity, wind speed, identifying materials, and acceleration, and can visualize the measurement data on an LCD display (Figure 14B). The device is also known as "electronic skin" because of its lightweight and is highly flexible, and its energy is entirely provided by a hand-shaped WTEG. The wearable application of environment detection focuses on protecting the health and safety of workers in dangerous places. Hand wearable devices are limited by the contact area of the thermoelectric devices and the skin and the volume of the wearable devices themselves, so the wearable applications in other parts have also

had great development. For example, Fazio et al. have developed a model to detect the wearer’s surrounding environment and its own biophysical parameters [120]. The system integrates heart rate ECG, accelerometer, temperature, and electrochemical gas sensors, using a flexible thermoelectric and solar power-combined power supply (Figure 14C). In addition, smart clothing is also equipped with a wireless communication port, which can realize information visualization and risk early warning by uploading the collected information to the mobile terminal or the cloud. The addition of the mobile IoT make wearables respond more quickly to collect information and further guarantees the health and safety of the wearer. In addition to the apps described above, MATRIX Co., Ltd. reported a man-powered smartwatch with multiple sensors built for movement tracking and health state measurement in 2020. It was able to interact with a phone and the cloud to support IOS and Android systems and is currently the only thermoelectric wearable product commercially available.

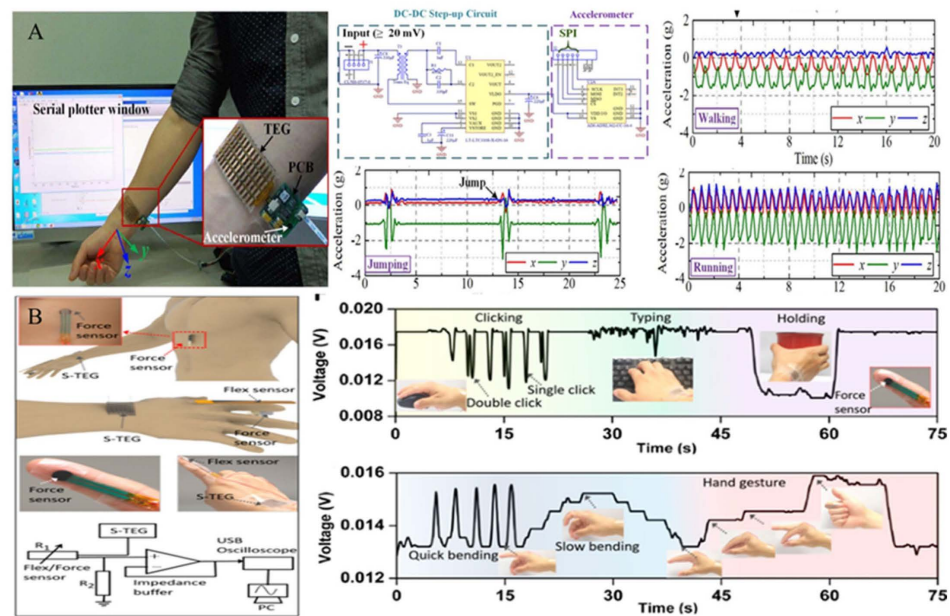


Figure 13. (A) Human movement state detection [58]. (B) Detection of hand activity [53].

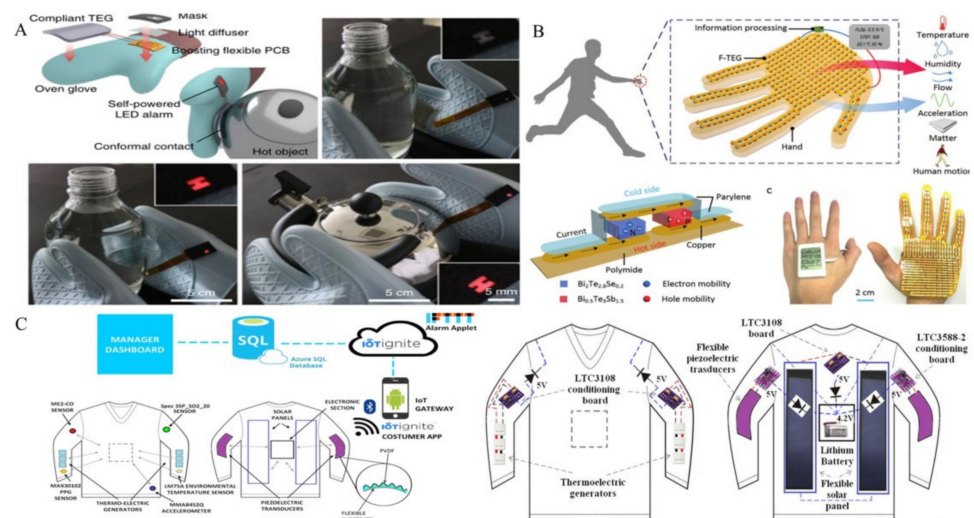


Figure 14. (A) Temperature detection device based on s-FTEG [76]. (B) A multifunctional detection system based on a palm-type thermoelectric generator [119]. (C) Intelligent clothing system [120].

Energy collection of wearable thermoelectrics is of great practical significance to the power supply of portable electronics for renewable energy when requiring light and sustainable work in fields such as medical, health, and environmental monitoring. In recent years, with the continuous improvement of the basic research on TE materials performance, the continuous realization of lower energy consumption and the flexibility of PCB, wearable thermoelectric generators have shown great potential in their application. In the future, as these technologies become more mature, combining the diversification of the IoT and the cloud, lighter, comfortable, and highly sensitive wearable devices will appear in our vision and life.

5. Conclusions and Challenges

Wearable thermoelectric generators (WTEGs) can incessantly convert body heat into electricity to power electronics. This review provides an overview of the technology for wearable thermoelectric generators based on inorganic bulk thermoelectric materials, from materials to device design and finally to applications. First, we explained the basic concepts and types of WTEGs. Because of WTEG's small-size, lightweight, no-noise, and reliability, it was used in the human body as a self-powered system, which is irreplaceable by other generators. Then, we introduced the popular inorganic bulk thermoelectric materials for WTEGs this year. Currently, most WTEGs use inorganic bulk thermocouples based on Bi_2Te_3 with high ZT to power wearable electronic devices. In addition, we also show the strategy of optimizing the output performance of TEG in recent years, the core content of which is to improve the temperature difference by optimizing the topology structure (geometry, connection, and heat dissipation) and fabricating process of the wearable thermoelectric generator while taking into account high reliability and flexibility. Besides r-WTEG and ns-FTEG, stretchable FTEGs have attracted a lot of attention in recent years because of their excellent flexibility and use in many special occasions. In applications, WTEG was used to power watches in the early days, but it has now been developed for various fields, such as biology and environment.

With the increasing market of wearable electronic devices, the development prospect and application market of efficient wearable thermoelectric generators are broad. As a relatively new field, wearable thermoelectric generators have made great progress in the past ten years, but nowadays, various wearable electronic devices with multi-function and high energy consumption require necessary properties of WTEG, such as high efficiency, durability, biological compatibility, and flexibility. In thermoelectric materials, high-efficiency thermoelectric generators require high ZT materials. Current thermoelectric materials and thermoelectric devices have not achieved satisfactory performance, so a lot of work is still needed in this research area. In general, Bi_2Te_3 exhibits superior TE performance at room temperature and can be mass-produced. Unfortunately, the development of wearable thermoelectric generators for human energy harvesting has been hindered by the inherent rigidity, toxicity, and danger of Bi_2Te_3 . Although Ag_2Se , MgAgSb , SnSe , and other non-toxic materials exhibit good performance at room temperature and show the potential to replace Bi_2Te_3 , there are still many challenges, such as TE properties, mechanical properties, cost, mass production, and reliability. In addition, heat sinks are a good strategy to improve device efficiency, but most of the flexible heat sinks designed for wearable thermoelectric generators are composed of thick hydrogels and copper plates, which do not take into account flexibility. Therefore, with the development of modern heat dissipation materials, such as graphene and radiant cooling, flexible, lightweight, and efficient wearable thermoelectric generators are expected. In order to solve the insufficient energy supply of self-powered wearable devices, the current trend is to combine a variety of wearable generators, such as solar power generators combined with thermoelectric and triboelectric nanogenerators. How to combine multiple wearable generators more effectively is also an urgent problem to be solved. In the future, the rapid development of new materials and technologies will bring greater application spaces and opportunities for wearable thermoelectric generators.

Author Contributions: Investigation, methodology, and writing—original draft preparation, S.Z.; investigation, Z.F., R.S., B.F. and Z.J.; conceptualization and supervision, Y.P. and J.G.; conceptualization, methodology, writing—review and editing, and supervision, L.M. and K.K. All authors have read and agreed to the published version of the manuscript.

Funding: This work was supported by the National Natural Science Foundation of China (grant no. U21A2054, 51961011, 52061009), the National Key Research and Development Program of China (no. 2017YFE9128000), and the Natural Science Foundation of Guangxi, China (grant no., 2021AC19206 and AD19110020).

Institutional Review Board Statement: Not applicable.

Informed Consent Statement: Not applicable.

Data Availability Statement: The data presented in this study are available on request from the corresponding author. The data are not publicly available due to confidentiality.

Acknowledgments: Not applicable.

Conflicts of Interest: The authors declare no conflict of interest.

References

1. Zhang, Y.; Shi, G.; Qin, J.; Lowe, S.E.; Zhang, S.; Zhao, H.; Zhong, Y.L. Recent Progress of Direct Ink Writing of Electronic Components for Advanced Wearable Devices. *ACS Appl. Electron. Mater.* **2019**, *1*, 1718–1734. [[CrossRef](#)]
2. Hu, X.; Li, F.; Song, Y. Wearable Power Source: A Newfangled Feasibility for Perovskite Photovoltaics. *ACS Energy Lett.* **2019**, *4*, 1065–1072. [[CrossRef](#)]
3. Jia, Y.; Jiang, Q.; Sun, H.; Liu, P.; Hu, D.; Pei, Y.; Liu, W.; Crispin, X.; Fabiano, S.; Ma, Y.; et al. Wearable Thermoelectric Materials and Devices for Self-Powered Electronic Systems. *Adv. Mater.* **2021**, *33*, e2102990. [[CrossRef](#)] [[PubMed](#)]
4. Yan, J.; Liao, X.; Yan, D.; Chen, Y. Review of Micro Thermoelectric Generator. *J. Microelectromech. Syst.* **2018**, *27*, 1–18. [[CrossRef](#)]
5. Haras, M.; Skotnicki, T. Thermoelectricity for IoT—A review. *Nano Energy* **2018**, *54*, 461–476. [[CrossRef](#)]
6. Gibson, J.S.; Liu, X.; Georgakopoulos, S.V.; Wie, J.J.; Ware, T.H.; White, T.J. Reconfigurable Antennas Based on Self-Morphing Liquid Crystalline Elastomers. *IEEE Access* **2016**, *4*, 2340–2348. [[CrossRef](#)]
7. Yang, Z.; Zhou, Q.; Lei, L.; Zheng, K.; Xiang, W. An IoT-cloud Based Wearable ECG Monitoring System for Smart Healthcare. *J. Med. Syst.* **2016**, *40*, 286. [[CrossRef](#)]
8. Guo, Z.; Ma, Y.; Dong, X.; Huang, J.; Wang, Y.; Xia, Y. An Environmentally Friendly and Flexible Aqueous Zinc Battery Using an Organic Cathode. *Angew. Chem. Int. Ed. Engl.* **2018**, *57*, 11737–11741. [[CrossRef](#)]
9. Zhang, S.S. Sulfurized Carbon: A Class of Cathode Materials for High Performance Lithium/Sulfur Batteries. *Front. Energy Res.* **2013**, *1*, 10. [[CrossRef](#)]
10. He, J.; Chen, Y.; Lv, W.; Wen, K.; Li, P.; Qi, F.; Wang, Z.; Zhang, W.; Li, Y.; Qin, W.; et al. Highly-flexible 3D Li₂S/graphene cathode for high-performance lithium sulfur batteries. *J. Power Sources* **2016**, *327*, 474–480. [[CrossRef](#)]
11. Starner, T. Human-powered wearable computing. *IEEE Access* **1996**, *35*, 618–629. [[CrossRef](#)]
12. Dieffenderfer, J.; Goodell, H.; Mills, S.; McKnight, M.; Yao, S.; Lin, F.; Beppler, E.; Bent, B.; Lee, B.; Misra, V.; et al. Low-Power Wearable Systems for Continuous Monitoring of Environment and Health for Chronic Respiratory Disease. *IEEE J. Biomed. Health Inform.* **2016**, *20*, 1251–1264. [[CrossRef](#)] [[PubMed](#)]
13. García Núñez, C.; Manjakkal, L.; Dahiya, R. Energy autonomous electronic skin. *npj Flex. Electron.* **2019**, *3*, 1. [[CrossRef](#)]
14. Huang, H.; Li, X.; Liu, S.; Hu, S.; Sun, Y. TriboMotion: A Self-Powered Triboelectric Motion Sensor in Wearable Internet of Things for Human Activity Recognition and Energy Harvesting. *IEEE Internet Things J.* **2018**, *5*, 4441–4453. [[CrossRef](#)]
15. Ha, M.; Park, J.; Lee, Y.; Ko, H. Triboelectric Generators and Sensors for Self-Powered Wearable Electronics. *ACS Nano* **2015**, *9*, 3421–3427. [[CrossRef](#)]
16. Wang, Z.L. On Maxwell's displacement current for energy and sensors: The origin of nanogenerators. *Mater. Today* **2017**, *20*, 74–82. [[CrossRef](#)]
17. Dong, K.; Peng, X.; An, J.; Wang, A.C.; Luo, J.; Sun, B.; Wang, J.; Wang, Z.L. Shape adaptable and highly resilient 3D braided triboelectric nanogenerators as e-textiles for power and sensing. *Nat. Commun.* **2020**, *11*, 2868. [[CrossRef](#)]
18. Chen, Z.; Wang, Z.; Li, X.; Lin, Y.; Luo, N.; Long, M.; Zhao, N.; Xu, J.B. Flexible Piezoelectric-Induced Pressure Sensors for Static Measurements Based on Nanowires/Graphene Heterostructures. *ACS Nano* **2017**, *11*, 4507–4513. [[CrossRef](#)]
19. Freer, R.; Powell, A.V. Realising the potential of thermoelectric technology: A Roadmap. *J. Mater. Chem. C* **2020**, *8*, 441–463. [[CrossRef](#)]
20. Soleimani, Z.; Zoras, S.; Ceranic, B.; Cui, Y.; Shahzad, S. A comprehensive review on the output voltage/power of wearable thermoelectric generators concerning their geometry and thermoelectric materials. *Nano Energy* **2021**, *89*, 106325. [[CrossRef](#)]
21. Zeng, W.; Tao, X.-M.; Lin, S.; Lee, C.; Shi, D.; Lam, K.-H.; Huang, B.; Wang, Q.; Zhao, Y. Defect-engineered reduced graphene oxide sheets with high electric conductivity and controlled thermal conductivity for soft and flexible wearable thermoelectric generators. *Nano Energy* **2018**, *54*, 163–174. [[CrossRef](#)]

22. Hasan, M.N.; Nafea, M.; Nayan, N.; Mohamed Ali, M.S. Thermoelectric Generator: Materials and Applications in Wearable Health Monitoring Sensors and Internet of Things Devices. *Adv. Mater. Technol.* **2021**, 2101203. [[CrossRef](#)]
23. Chen, G.; Xu, W.; Zhu, D. Recent advances in organic polymer thermoelectric composites. *J. Mater. Chem. C* **2017**, *5*, 4350–4360. [[CrossRef](#)]
24. Elmoughni, H.M.; Menon, A.K.; Wolfe, R.M.W.; Yee, S.K. A Textile-Integrated Polymer Thermoelectric Generator for Body Heat Harvesting. *Adv. Mater. Technol.* **2019**, *4*, 1800708. [[CrossRef](#)]
25. Wang, H.; Yu, C. Organic Thermoelectrics: Materials Preparation, Performance Optimization, and Device Integration. *Joule* **2019**, *3*, 53–80. [[CrossRef](#)]
26. Cui, Y.J.; Wang, B.L.; Wang, K.F. Energy conversion performance optimization and strength evaluation of a wearable thermoelectric generator made of a thermoelectric layer on a flexible substrate. *Energy* **2021**, *229*, 120694. [[CrossRef](#)]
27. Bharti, M.; Singh, A.; Singh, B.P.; Dhakate, S.R.; Saini, G.; Bhattacharya, S.; Debnath, A.K.; Muthe, K.P.; Aswal, D.K. Free-standing flexible multiwalled carbon nanotubes paper for wearable thermoelectric power generator. *J. Power Sources* **2020**, *449*, 227493. [[CrossRef](#)]
28. Chen, Z.; Lv, H.; Zhang, Q.; Wang, H.; Chen, G. Construction of a cement–rebar nanoarchitecture for a solution-processed and flexible film of a Bi₂Te₃/CNT hybrid toward low thermal conductivity and high thermoelectric performance. *Carbon Energy* **2021**, *4*, 115–128. [[CrossRef](#)]
29. DiSalvo, F.J. Thermoelectric cooling and power generation. *Science* **1999**, *285*, 703–706. [[CrossRef](#)]
30. Majumdar, A. Materials science. Thermoelectricity in semiconductor nanostructures. *Science* **2004**, *303*, 777–778. [[CrossRef](#)]
31. Toberer, G.J.S.E.S. Complex thermoelectric materials. *Nat. Mater.* **2008**, *7*, 105–114.
32. Rosi, F.D. Thermoelectricity and thermoelectric power generation. *Solid-State Electron.* **1968**, *11*, 833–868. [[CrossRef](#)]
33. Selvan, K.V.; Hasan, M.N.; Mohamed Ali, M.S. State-of-the-Art Reviews and Analyses of Emerging Research Findings and Achievements of Thermoelectric Materials over the Past Years. *J. Electron. Mater.* **2018**, *48*, 745–777. [[CrossRef](#)]
34. Selvan, K.V.; Hasan, M.N.; Mohamed Ali, M.S. Methodological reviews and analyses on the emerging research trends and progresses of thermoelectric generators. *Int. J. Energy Res.* **2018**, *43*, 113–140. [[CrossRef](#)]
35. Rowe, D.M. *Thermoelectrics Handbook*; CRC Press: Boca Raton, FL, USA, 2006.
36. Zoui, M.A.; Bentouba, S.; Stocholm, J.G.; Bourouis, M. A Review on Thermoelectric Generators: Progress and Applications. *Energies* **2020**, *13*, 3606. [[CrossRef](#)]
37. Lee, Y.G.; Kim, J.; Kang, M.-S.; Baek, S.-H.; Kim, S.K.; Lee, S.-M.; Lee, J.; Hyun, D.-B.; Ju, B.-K.; Moon, S.E.; et al. Design and Experimental Investigation of Thermoelectric Generators for Wearable Applications. *Adv. Mater. Technol.* **2017**, *2*, 1600292. [[CrossRef](#)]
38. Nozariasbmarz, A.; Collins, H.; Dsouza, K.; Polash, M.H.; Hosseini, M.; Hyland, M.; Liu, J.; Malhotra, A.; Ortiz, F.M.; Mohaddes, F.; et al. Review of wearable thermoelectric energy harvesting: From body temperature to electronic systems. *Appl. Energy* **2020**, *258*, 114069. [[CrossRef](#)]
39. Leonov, V.; Vullers, R.J.M. Thermoelectric Generators on Living Beings. In Proceedings of the 5th European Conference on Thermoelectrics (ECT 2007), Odessa, Ukraine, 10–12 September 2007.
40. Webb, P. Temperatures of skin, subcutaneous tissue, muscle and core in resting men in cold, comfortable and hot conditions. *Appl. Physiol.* **1992**, *64*, 471–476. [[CrossRef](#)]
41. Saggin, B.; Tarabini, M.; Lanfranchi, G. A Device for the Skin–Contact Thermal Resistance Measurement. *IEEE Trans. Instrum. Meas.* **2012**, *61*, 489–495. [[CrossRef](#)]
42. Ho, H.N.; Jones, L.A. Thermal model for hand-object interactions. In Proceedings of the 2006 14th Symposium on Haptic Interfaces for Virtual Environment and Teleoperator Systems, Alexandria, VA, USA, 25–26 March 2006; pp. 461–467.
43. Mori, Y.; Kioka, E.; Tokura, H. Effects of pressure on the skin exerted by clothing on responses of urinary catecholamines and cortisol, heart rate and nocturnal urinary melatonin in humans. *Int. J. Biometeorol.* **2002**, *47*, 1–5. [[CrossRef](#)]
44. Suarez, F.; Nozariasbmarz, A.; Vashae, D.; Öztürk, M.C. Designing thermoelectric generators for self-powered wearable electronics. *Energy Environ. Sci.* **2016**, *9*, 2099–2113. [[CrossRef](#)]
45. Qi, Y.; McAlpine, M.C. Nanotechnology-enabled flexible and biocompatible energy harvesting. *Energy Environ. Sci.* **2010**, *3*, 1275–1285. [[CrossRef](#)]
46. Leonov, V.; Torfs, T.; Fiorini, P.; Van Hoof, C. Thermoelectric Converters of Human Warmth for Self-Powered Wireless Sensor Nodes. *IEEE Sens. J.* **2007**, *7*, 650–657. [[CrossRef](#)]
47. Settaluri, K.T.; Lo, H.; Ram, R.J. Thin Thermoelectric Generator System for Body Energy Harvesting. *J. Electron. Mater.* **2011**, *41*, 984–988. [[CrossRef](#)]
48. Nozariasbmarz, A.; Kishore, R.A.; Poudel, B.; Saparamadu, U.; Li, W.; Cruz, R.; Priya, S. High Power Density Body Heat Energy Harvesting. *ACS Appl. Mater. Interfaces* **2019**, *11*, 40107–40113. [[CrossRef](#)]
49. Yuan, J.; Zhu, R. A fully self-powered wearable monitoring system with systematically optimized flexible thermoelectric generator. *Appl. Energy* **2020**, *271*, 115250. [[CrossRef](#)]
50. Kim, S.J.; We, J.H.; Cho, B.J. A wearable thermoelectric generator fabricated on a glass fabric. *Energy Environ. Sci.* **2014**, *7*, 1959–1965. [[CrossRef](#)]

51. Park, H.; Lee, D.; Kim, D.; Cho, H.; Eom, Y.; Hwang, J.; Kim, H.; Kim, J.; Han, S.; Kim, W. High power output from body heat harvesting based on flexible thermoelectric system with low thermal contact resistance. *J. Phys. D Appl. Phys.* **2018**, *51*, 365501. [[CrossRef](#)]
52. Zadan, M.; Malakooti, M.H.; Majidi, C. Soft and Stretchable Thermoelectric Generators Enabled by Liquid Metal Elastomer Composites. *ACS Appl. Mater. Interfaces* **2020**, *12*, 17921–17928. [[CrossRef](#)]
53. Yang, Y.; Hu, H.; Chen, Z.; Wang, Z.; Jiang, L.; Lu, G.; Li, X.; Chen, R.; Jin, J.; Kang, H.; et al. Stretchable Nanolayered Thermoelectric Energy Harvester on Complex and Dynamic Surfaces. *Nano Lett.* **2020**, *20*, 4445–4453. [[CrossRef](#)]
54. Hyland, M.; Hunter, H.; Liu, J.; Veety, E.; Vashaee, D. Wearable thermoelectric generators for human body heat harvesting. *Appl. Energy* **2016**, *182*, 518–524. [[CrossRef](#)]
55. Nozariasbmarz, A.; Suarez, F.; Dycus, J.H.; Cabral, M.J.; LeBeau, J.M.; Öztürk, M.C.; Vashaee, D. Thermoelectric generators for wearable body heat harvesting: Material and device concurrent optimization. *Nano Energy* **2020**, *67*, 104265. [[CrossRef](#)]
56. Jo, S.E.; Kim, M.K.; Kim, M.S.; Kim, Y.J. Flexible thermoelectric generator for human body heat energy harvesting. *Electron. Lett.* **2012**, *48*, 1015–1017. [[CrossRef](#)]
57. Shi, Y.; Wang, Y.; Mei, D.; Feng, B.; Chen, Z. Design and Fabrication of Wearable Thermoelectric Generator Device for Heat Harvesting. *IEEE Rob. Autom. Lett.* **2018**, *3*, 373–378. [[CrossRef](#)]
58. Wang, Y.; Shi, Y.; Mei, D.; Chen, Z. Wearable thermoelectric generator to harvest body heat for powering a miniaturized accelerometer. *Appl. Energy* **2018**, *215*, 690–698. [[CrossRef](#)]
59. Kim, C.S.; Lee, G.S.; Choi, H.; Kim, Y.J.; Yang, H.M.; Lim, S.H.; Lee, S.-G.; Cho, B.J. Structural design of a flexible thermoelectric power generator for wearable applications. *Appl. Energy* **2018**, *214*, 131–138. [[CrossRef](#)]
60. Suarez, F.; Parekh, D.P.; Ladd, C.; Vashaee, D.; Dickey, M.D.; Öztürk, M.C. Flexible thermoelectric generator using bulk legs and liquid metal interconnects for wearable electronics. *Appl. Energy* **2017**, *202*, 736–745. [[CrossRef](#)]
61. Hong, S.; Gu, Y.; Seo, J.K.; Wang, J.; Liu, P.; Meng, Y.S.; Xu, S.; Chen, R. Wearable thermoelectrics for personalized thermoregulation. *Sci. Adv.* **2019**, *5*, eaaw0536. [[CrossRef](#)]
62. Sargolzaeiaval, Y.; Padmanabhan Ramesh, V.; Neumann, T.V.; Misra, V.; Vashaee, D.; Dickey, M.D.; Öztürk, M.C. Flexible thermoelectric generators for body heat harvesting—Enhanced device performance using high thermal conductivity elastomer encapsulation on liquid metal interconnects. *Appl. Energy* **2020**, *262*, 114370. [[CrossRef](#)]
63. Ramesh, V.P.; Sargolzaeiaval, Y.; Neumann, T.; Misra, V.; Vashaee, D.; Dickey, M.D.; Öztürk, M.C. Flexible thermoelectric generator with liquid metal interconnects and low thermal conductivity silicone filler. *npj Flex. Electron.* **2021**, *5*, 5. [[CrossRef](#)]
64. Zhu, S.; Peng, Y.; Gao, J.; Miao, L.; Lai, H.; Liu, C.; Zhang, J.; Zhang, Y.; Zhou, S.; Koumoto, K.; et al. Simultaneous Realization of Flexibility and Ultrahigh Normalized Power Density in a Heatsink-Free Thermoelectric Generator via Fine Thermal Regulation. *ACS Appl. Mater. Interfaces* **2022**, *14*, 1045–1055. [[CrossRef](#)]
65. Lee, D.; Park, H.; Park, G.; Kim, J.; Kim, H.; Cho, H.; Han, S.; Kim, W. Liquid-metal-electrode-based compact, flexible, and high-power thermoelectric device. *Energy* **2019**, *188*, 116019. [[CrossRef](#)]
66. Park, H.; Kim, D.; Eom, Y.; Wijethunge, D.; Hwang, J.; Kim, H.; Kim, W. Mat-like flexible thermoelectric system based on rigid inorganic bulk materials. *J. Phys. D Appl. Phys.* **2017**, *50*, 494006. [[CrossRef](#)]
67. Eom, Y.; Wijethunge, D.; Park, H.; Park, S.H.; Kim, W. Flexible thermoelectric power generation system based on rigid inorganic bulk materials. *Appl. Energy* **2017**, *206*, 649–656. [[CrossRef](#)]
68. Xu, Q.; Deng, B.; Zhang, L.; Lin, S.; Han, Z.; Zhou, Q.; Li, J.; Zhu, Y.; Jiang, F.; Li, Q.; et al. High-performance, flexible thermoelectric generator based on bulk materials. *Cell Rep. Phys. Sci.* **2022**, *3*, 100780. [[CrossRef](#)]
69. Kim, J.; Khan, S.; Wu, P.; Park, S.; Park, H.; Yu, C.; Kim, W. Self-charging wearables for continuous health monitoring. *Nano Energy* **2021**, *79*, 105419. [[CrossRef](#)]
70. Jung, S.-J.; Shin, J.; Lim, S.-S.; Kwon, B.; Baek, S.-H.; Kim, S.K.; Park, H.-H.; Kim, J.-S. Porous organic filler for high efficiency of flexible thermoelectric generator. *Nano Energy* **2021**, *81*, 105604. [[CrossRef](#)]
71. Kim, C.S.; Yang, H.M.; Lee, J.; Lee, G.S.; Choi, H.; Kim, Y.J.; Lim, S.H.; Cho, S.H.; Cho, B.J. Self-Powered Wearable Electrocardiography Using a Wearable Thermoelectric Power Generator. *ACS Energy Lett.* **2018**, *3*, 501–507. [[CrossRef](#)]
72. Khan, S.; Kim, J.; Roh, K.; Park, G.; Kim, W. High power density of radiative-cooled compact thermoelectric generator based on body heat harvesting. *Nano Energy* **2021**, *87*, 10618. [[CrossRef](#)]
73. Liu, Y.; Yin, L.; Zhang, W.; Wang, J.; Hou, S.; Wu, Z.; Zhang, Z.; Chen, C.; Li, X.; Ji, H.; et al. A wearable real-time power supply with a Mg₃Bi₂-based thermoelectric module. *Cell Rep. Phys. Sci.* **2021**, *2*, 100412. [[CrossRef](#)]
74. Lee, G.; Kim, C.S.; Kim, S.; Kim, Y.J.; Choi, H.; Cho, B.J. Flexible heatsink based on a phase-change material for a wearable thermoelectric generator. *Energy* **2019**, *179*, 12–18. [[CrossRef](#)]
75. Hou, Y.; Yang, Y.; Wang, Z.; Li, Z.; Zhang, X.; Bethers, B.; Xiong, R.; Guo, H.; Yu, H. Whole Fabric-Assisted Thermoelectric Devices for Wearable Electronics. *Adv. Sci.* **2022**, *9*, 2103574. [[CrossRef](#)] [[PubMed](#)]
76. Lee, B.; Cho, H.; Park, K.T.; Kim, J.S.; Park, M.; Kim, H.; Hong, Y.; Chung, S. High-performance compliant thermoelectric generators with magnetically self-assembled soft heat conductors for self-powered wearable electronics. *Nat. Commun.* **2020**, *11*, 5948. [[CrossRef](#)] [[PubMed](#)]
77. Peng, Y.; Miao, L.; Liu, C.; Song, H.; Kurosawa, M.; Nakatsuka, O.; Back, S.Y.; Rhyee, J.S.; Murata, M.; Tanemura, S.; et al. Constructed Ge Quantum Dots and Sn Precipitate SiGeSn Hybrid Film with High Thermoelectric Performance at Low Temperature Region. *Adv. Energy Mater.* **2021**, *12*, 2103191. [[CrossRef](#)]

78. Gorai, P.; Stevanović, V.; Toberer, E.S. Computationally guided discovery of thermoelectric materials. *Nat. Rev. Mater.* **2017**, *2*, 17053. [[CrossRef](#)]
79. Wu, Z.; Zhang, S.; Liu, Z.; Mu, E.; Hu, Z. Thermoelectric converter: Strategies from materials to device application. *Nano Energy* **2022**, *91*, 106692. [[CrossRef](#)]
80. Hong, M.; Chasapis, T.C.; Chen, Z.G.; Yang, L.; Kanatzidis, M.G.; Snyder, G.J.; Zou, J. n-Type Bi₂Te₃-xSex Nanoplates with Enhanced Thermoelectric Efficiency Driven by Wide-Frequency Phonon Scatterings and Synergistic Carrier Scatterings. *ACS Nano* **2016**, *10*, 4719–4727. [[CrossRef](#)]
81. Hong, M.; Chen, Z.-G.; Zou, J. Fundamental and progress of Bi₂Te₃-based thermoelectric materials. *Chin. Phys. B* **2018**, *27*, 048403. [[CrossRef](#)]
82. Parás-Hernández, F.U.; Fabián-Mijangos, A.; Cardona-Castro, M.A.; Alvarez-Quintana, J. Enhanced performance nanostructured thermoelectric converter for self-powering health sensors. *Nano Energy* **2020**, *74*, 104854. [[CrossRef](#)]
83. Liu, C.-J.; Lai, H.C.; Liu, Y.-L.; Chen, L.-R. High thermoelectric figure-of-merit in p-type nanostructured (Bi,Sb)₂Te₃ fabricated via hydrothermal synthesis and evacuated-and-encapsulated sintering. *J. Mater. Chem.* **2012**, *22*, 4825–4831. [[CrossRef](#)]
84. Jun, P. Preparation and Characterization of Telluride Based Thermoelectric Materials and Device. Ph.D. Thesis, University of Science and Technology Beijing, Beijing, China, 2019.
85. Zhen, Y. The Fabrication and Mechanical Performance of p-Type Bismuth Telluride-Based Thermoelectric Materials. Ph.D. Thesis, Wuhan University of Technology, Wuhan, China, 2015.
86. Kim, S.I.; Lee, K.H.; Mun, H.A.; Kim, H.S.; Hwang, S.W.; Roh, J.W.; Yang, D.J.; Shin, W.H.; Li, X.S.; Lee, Y.H.; et al. Dense dislocation arrays embedded in grain boundaries for high-performance bulk thermoelectrics. *Science* **2015**, *348*, 109–114. [[CrossRef](#)] [[PubMed](#)]
87. Poudel, B.; Hao, Q.; Ma, Y.; Lan, Y.; Minnich, A.; Yu, B.; Yan, X.; Wang, D.; Muto, A.; Vashaee, D. High-Thermoelectric Performance of Nanostructured Bismuth Antimony Telluride Bulk Alloys. *Science* **2008**, *320*, 634–638. [[CrossRef](#)] [[PubMed](#)]
88. Nozariasbmarz, A.; Vashaee, D. Effect of Microwave Processing and Glass Inclusions on Thermoelectric Properties of P-Type Bismuth Antimony Telluride Alloys for Wearable Applications. *Energies* **2020**, *13*, 4524. [[CrossRef](#)]
89. Venkatasubramanian, R.; Siivola, E.; Colpitts, T.; O’Quinn, B. Thin-film thermoelectric devices with high room-temperature figures of merit. *Nature* **2001**, *413*, 597–602. [[CrossRef](#)]
90. Lu, Y.; Qiu, Y.; Cai, K.; Ding, Y.; Wang, M.; Jiang, C.; Yao, Q.; Huang, C.; Chen, L.; He, J. Ultrahigh power factor and flexible silver selenide-based composite film for thermoelectric devices. *Energy Environ. Sci.* **2020**, *13*, 1240–1249. [[CrossRef](#)]
91. Gao, W.; Yi, X.; Cui, B.; Wang, Z.; Huang, J.; Sui, J.; Liu, Z. The critical role of boron doping in the thermoelectric and mechanical properties of nanostructured α -MgAgSb. *J. Mater. Chem. C* **2018**, *6*, 9821–9827. [[CrossRef](#)]
92. Zhang, T.; Dong, B.; Wang, X. Optimization of the thermoelectric performance of α -MgAgSb-based materials by Zn-doping. *J. Mater. Sci.* **2021**, *56*, 13715–13722. [[CrossRef](#)]
93. Zheng, Y.; Liu, C.; Miao, L.; Li, C.; Huang, R.; Gao, J.; Wang, X.; Chen, J.; Zhou, Y.; Nishibori, E. Extraordinary thermoelectric performance in MgAgSb alloy with ultralow thermal conductivity. *Nano Energy* **2019**, *59*, 311–320. [[CrossRef](#)]
94. Zhou, C.; Lee, Y.K.; Yu, Y.; Byun, S.; Luo, Z.Z.; Lee, H.; Ge, B.; Lee, Y.L.; Chen, X.; Lee, J.Y.; et al. Polycrystalline SnSe with a thermoelectric figure of merit greater than the single crystal. *Nat. Mater.* **2021**, *20*, 1378–1384. [[CrossRef](#)]
95. Chen, Z.-G.; Shi, X.; Zhao, L.-D.; Zou, J. High-performance SnSe thermoelectric materials: Progress and future challenge. *Prog. Mater. Sci.* **2018**, *97*, 283–346. [[CrossRef](#)]
96. Su, L.; Wang, D.; Wang, S.; Qin, B.; Wang, Y.; Qin, Y.; Jin, Y.; Chang, C.; Zhao, L.-D. High thermoelectric performance realized through manipulating layered phonon-electron decoupling. *Science* **2022**, *375*, 1385–1389. [[CrossRef](#)] [[PubMed](#)]
97. Zhao, L.-D.; Tan, G.; Hao, S.; He, J.; Pei, Y.; Chi, H.; Wang, H.; Gong, S.; Xu, H.; Dravid, V.P.; et al. Ultrahigh power factor and thermoelectric performance in hole-doped single-crystal SnSe. *Science* **2015**, *351*, 141–144. [[CrossRef](#)] [[PubMed](#)]
98. Deng, S.; Jiang, X.; Chen, L.; Qi, N.; Tang, X.; Chen, Z. Ultralow Thermal Conductivity and High Thermoelectric Performance in AgCuTe_{1-x}Sex through Isoelectronic Substitution. *ACS Appl. Mater. Interfaces* **2021**, *13*, 868–877. [[CrossRef](#)] [[PubMed](#)]
99. Jiang, J.; Zhu, H.; Niu, Y.; Zhu, Q.; Song, S.; Zhou, T.; Wang, C.; Ren, Z. Achieving high room-temperature thermoelectric performance in cubic AgCuTe. *J. Mater. Chem. A* **2020**, *8*, 4790–4799. [[CrossRef](#)]
100. Gao, J.; Miao, L.; Liu, C.; Wang, X.; Peng, Y.; Wei, X.; Zhou, J.; Chen, Y.; Hashimoto, R.; Asaka, T.; et al. A novel glass-fiber-aided cold-press method for fabrication of n-type Ag₂Te nanowires thermoelectric film on flexible copy-paper substrate. *J. Mater. Chem. A* **2017**, *5*, 24740–24748. [[CrossRef](#)]
101. Zhong, Y.; Tang, J.; Liu, H.; Chen, Z.; Lin, L.; Ren, D.; Liu, B.; Ang, R. Optimized Strategies for Advancing n-Type PbTe Thermoelectrics: A Review. *ACS Appl. Mater. Interfaces* **2020**, *12*, 49323–49334. [[CrossRef](#)]
102. Zhao, H.; Sui, J.; Tang, Z.; Lan, Y.; Jie, Q.; Kraemer, D.; McEnaney, K.; Guloy, A.; Chen, G.; Ren, Z. High thermoelectric performance of MgAgSb-based materials. *Nano Energy* **2014**, *7*, 97–103. [[CrossRef](#)]
103. Lei, J.; Zhang, D.; Guan, W.; Ma, Z.; Cheng, Z.; Wang, C.; Wang, Y. Enhancement of thermoelectric figure of merit by the insertion of multi-walled carbon nanotubes in α -MgAgSb. *Appl. Phys. Lett.* **2018**, *113*, 083901. [[CrossRef](#)]
104. Wang, H.; Liu, X.; Zhou, Z.; Wu, H.; Chen, Y.; Zhang, B.; Wang, G.; Zhou, X.; Han, G. Constructing n-type Ag₂Se/CNTs composites toward synergistically enhanced thermoelectric and mechanical performance. *Acta Mater.* **2022**, *223*, 117502. [[CrossRef](#)]
105. Day, T.; Drymiotis, F.; Zhang, T.; Rhodes, D.; Shi, X.; Chen, L.; Snyder, G.J. Evaluating the potential for high thermoelectric efficiency of silver selenide. *J. Mater. Chem. C* **2013**, *1*, 7568–7573. [[CrossRef](#)]

106. Jood, P.; Chetty, R.; Ohta, M. Structural stability enables high thermoelectric performance in room temperature Ag₂Se. *J. Mater. Chem. A* **2020**, *8*, 13024–13037. [[CrossRef](#)]
107. Jiang, C.; Ding, Y.; Cai, K.; Tong, L.; Lu, Y.; Zhao, W.; Wei, P. Ultrahigh Performance of n-Type Ag₂Se Films for Flexible Thermoelectric Power Generators. *ACS Appl. Mater. Interfaces* **2020**, *12*, 9646–9655. [[CrossRef](#)] [[PubMed](#)]
108. Chen, J.; Liu, T.; Bao, D.; Zhang, B.; Han, G.; Liu, C.; Tang, J.; Zhou, D.; Yang, L.; Chen, Z.G. Nanostructured monoclinic Cu₂Se as a near-room-temperature thermoelectric material. *Nanoscale* **2020**, *12*, 20536–20542. [[CrossRef](#)] [[PubMed](#)]
109. Liu, Y.; Shi, Y.; Li, J.; Guo, X.; Wang, Y.; Xiang, Q.; Guo, S.; Ze, R.; Zeng, J.; Xiang, Y.; et al. Comprehensive performance prediction and power promotion for wearable thermoelectric generator with flexible encapsulation in practical application. *Energy Convers. Manag.* **2020**, *220*, 113080. [[CrossRef](#)]
110. Tanwar, A.; Lal, S.; Razeeb, K. Structural Design Optimization of Micro-Thermoelectric Generator for Wearable Biomedical Devices. *Energies* **2021**, *14*, 2339. [[CrossRef](#)]
111. Leonov, V.; Vullers, R.J.M. Wearable Thermoelectric Generators for Body-Powered Devices. *J. Electron. Mater.* **2009**, *38*, 1491–1498. [[CrossRef](#)]
112. Zhu, K.; Deng, B.; Zhang, P.; Kim, H.S.; Jiang, P.; Liu, W. System efficiency and power: The bridge between the device and system of a thermoelectric power generator. *Energy Environ. Sci.* **2020**, *13*, 3514–3526. [[CrossRef](#)]
113. Pietrzyk, K.; Soares, J.; Ohara, B.; Lee, H. Power generation modeling for a wearable thermoelectric energy harvester with practical limitations. *Appl. Energy* **2016**, *183*, 218–228. [[CrossRef](#)]
114. Elghool, A.; Basrawi, F.; Ibrahim, T.K.; Habib, K.; Ibrahim, H.; Idris, D.M.N.D. A review on heat sink for thermo-electric power generation: Classifications and parameters affecting performance. *Energy Convers. Manag.* **2017**, *134*, 260–277. [[CrossRef](#)]
115. Kim, S.J.; Lee, H.E.; Choi, H.; Kim, Y.; We, J.H.; Shin, J.S.; Lee, K.J.; Cho, B.J. High-Performance Flexible Thermoelectric Power Generator Using Laser Multiscanning Lift-Off Process. *ACS Nano* **2016**, *10*, 10851–10857. [[CrossRef](#)]
116. Thermoelectric Generator Market. Thermoelectric Generator Market by Material, Application, and End-use Industry: Global Opportunity Analysis and Industry Forecast, 2021–2030. Available online: <https://www.researchandmarkets.com/reports/5521526/thermoelectric-generator-market-by-material#> (accessed on 5 February 2022).
117. Tom Torfs, V.L. Ruud Vullers, Pulse Oximeter Fully Powered by Human Body Heat. *Sens. Transducers* **2007**, *80*, 1230–1238.
118. Lay-Ekuakille, A.; Vendramin, G.; Trotta, A.; Mazzotta, G. Thermoelectric Generator Design Based on Power from Body Heat for Biomedical Autonomous Devices. In *International Workshop on Medical Measurements and Applications*; IEEE: Cetraro, Italy, 2009.
119. Yuan, J.; Zhu, R.; Li, G. Self-Powered Electronic Skin with Multisensory Functions Based on Thermoelectric Conversion. *Adv. Mater. Technol.* **2020**, 2000419. [[CrossRef](#)]
120. de Fazio, R.; Cafagna, D.; Marcuccio, G.; Minerba, A.; Visconti, P. A Multi-Source Harvesting System Applied to Sensor-Based Smart Garments for Monitoring Workers' Bio-Physical Parameters in Harsh Environments. *Energies* **2020**, *13*, 2161. [[CrossRef](#)]